

# Particulate Rare Earth Element behavior in the North Atlantic (GEOVIDE cruise)

Marion Lagarde<sup>1</sup>, Nolwenn Lemaitre<sup>2</sup>, H el ene Planquette<sup>3</sup>, M elanie Grenier<sup>1</sup>, Moustafa Belhadj<sup>1</sup>, Pascale Lherminier<sup>4</sup>, Catherine Jeandel<sup>1</sup>

5 <sup>1</sup> LEGOS, University of Toulouse, CNRS, CNES, IRD, UPS, Toulouse, 31400, France

<sup>2</sup> ETH, Zurich, IGP, Zurich, Switzerland

<sup>3</sup> LEMAR, University of Brest, CNRS, IRD, Ifremer, Plouzan e, 29280, France

<sup>4</sup> LOPS, Ifremer, CNRS, IRD, UBO, Ifremer, Plouzan e, 29280, France

*Correspondence to:* Marion Lagarde (marion.lagarde@legos.obs-mip.fr)

10 **Abstract.** Particulate concentrations of the fourteen Rare Earth Elements (PREE), yttrium and 232-thorium were measured in 200 samples collected in the epipelagic (ca 0-200 m) and the mesopelagic (ca 200-1500 m) zones of the North Atlantic, during the GEOVIDE cruise (May/June 2014, R/V Pourquoi Pas?, GEOTRACES GA01), [providing the most detailed snapshot of the PREE distribution in the North Atlantic so far](#). Concentrations of particulate cerium (PCe) varied between 0.2 pmol L<sup>-1</sup> and 16 pmol L<sup>-1</sup>, while particulate neodymium (PNd) concentrations ranged between 0.1 pmol L<sup>-1</sup> and 6.1 pmol L<sup>-1</sup>. Particulate  
15 ytterbium (PYb) concentrations ranged between 0.01 pmol L<sup>-1</sup> and 0.50 pmol L<sup>-1</sup>. In addition, this study showed that PREE distributions were also controlled by the biological production in the upper sunlit ocean and by remineralization processes in the mesopelagic area. Low surface concentrations combined with normalized PREE patterns displaying a negative Ce anomaly and HREE enrichments pointed to freshly formed biogenic particles [imprinting the seawater signature](#). A significant relationship between biogenic silica (BSi) and PHREE was also observed in the Labrador and Irminger Seas, due to the  
20 occurrence of strong diatom blooms at the sampling time. In order to identify dissolved-particulate processes independent of the ionic radius, we used PHo/PY ratios and showed that [absorption processes were predominant in the upper ocean while adsorption processes dominated at deeper depths](#).

This study highlighted different lithogenic fractions of PREE and dispersion depending on the shelf: off the Iberian margin, up to 100% of the PREE were determined to have a lithogenic origin. This lithogenic input spread westward along an  
25 intermediate nepheloid layer (INL), following isopycnals up to 1700 km away from the margin. In contrast, along the Greenland and Newfoundland margins, the circulation maintained lithogenic inputs of PREE along the coasts.

## 1 Introduction

30 [Particles and water mass circulation are the main vectors in transferring chemical species from the surface to the deep ocean](#) (Gehlen et al., 2006; Kwon et al., 2009; Lam and Marchal, 2015; Ohnemus and Lam, 2015). Particles are abundant in the upper ocean (up to 1000 µg L<sup>-1</sup>), where dust inputs or important blooms occur, and their concentration decrease with depth in the

subsurface and deep ocean (5 to 60  $\mu\text{g L}^{-1}$  on average, McCave and Hall, 2002; Stemmann et al., 2002). Particles are usually divided in two classes: large sinking particles that dominate the vertical flux, and small particles that are in suspension in the water column. These small suspended particles represent over 80% of the total particle mass (Lam et al., 2015 and references therein). In addition, their higher surface to volume ratios make suspended particles the main drivers of dissolved-particulate exchanges (Crececius, 1980; Trull and Armand, 2001). Elements are up to 1000 times more concentrated in particles than in the dissolved phase (Lam et al., 2015), and among them trace metals are especially enriched in particles. For example, in the subpolar North Atlantic, particulate iron (PFe) concentrations can reach 50  $\text{nmol L}^{-1}$  while dissolved Fe concentrations does not exceed 2.5  $\text{nmol L}^{-1}$  (Tonnard et al., 2020). As the size spectrum between the particulate and the dissolved phase is continuous, the separation between the two pools is truly operational, based on the porosity of the filters used to discriminate the two phases, usually 0.4  $\mu\text{m}$  (Planquette and Sherrell, 2012). Concentrations may then depend on the choice of this limit.

In the ocean, three main sources of particles are distinguishable (Fowler and Knauer, 1986; Jeandel et al., 2015; Lam et al., 2015 and references therein). The first one is lithogenic, with inputs from the rivers, dust deposits, ice melting and resuspension of deposited sediments. The second is biogenic, and related to the production of fresh organic matter by photosynthetic activity followed by zooplankton grazing, and the following food web activity. The last one results from authigenic processes such as the precipitation and formation of red clays, oxides and hydroxides. All these sources and processes lead to a very heterogeneous pool, in time, space and composition, evolving throughout their stay in the ocean and controlling the density of particles, and consequently their fate in the water column. Then, exchanges between the particulate and dissolved phases determine the chemistry of seawater and the residence time of the chemical species in the ocean (Jeandel et al., 2015; Jeandel and Oelkers, 2015; Turekian, 1977).

Oceanic tracers such as rare earth elements (REE) are adapted to the study of these exchanges (Jeandel et al., 1995; Kuss et al., 2001; Tachikawa et al., 1999b). Rare earth elements form a homogenous family characterized by a gradual filling of the 4f orbital as their atomic number increase. Except for cerium (Ce), their external orbital comprises three electrons, rendering their chemical properties relatively similar. However, the increasing weight concomitant with an increasing atomic number and the decreasing ionic radius generates slight differences between the light and heavy REE behaviors (LREE and HREE respectively). In seawater REE are mostly complexed by carbonates, this complexation increasing with the atomic number: 86% of lanthanum (La, the first REE of the series) is found as carbonates complexes, while this proportion is 99% of lutetium (Lu, the last REE of the series) (Schijf et al., 2015). Thus, the REE will react differently in the water column depending on various physical and geochemical processes such as aggregation-disaggregation, dissolution, complexation, sorption, mineralization and scavenging. These processes will lead to a fractionation along the REE series. Consequently, measuring the distribution of REEs between the solid and dissolved phases can help tracing and quantifying these processes.

Documenting these exchanges in the subarctic North Atlantic using REE among other tracers was one of the goals of the GEOVIDE cruise (2014, GA01 GEOTRACES cruise; Fig. 1). The North Atlantic is a key region of the global ocean, as it is the most important oceanic sink of anthropogenic  $\text{CO}_2$  (Khawala et al., 2013), and it is i) a major place of deep water formation, mainly by convection, which drives the Atlantic meridional overturning circulation (AMOC), and ii) a productive

area, representing up to 18% of the global oceanic primary production (Sanders et al., 2014). The GEOVIDE section investigated stations close to the Iberian, Greenland and Canadian coasts and crossed areas of contrasted surface productivity. This cruise was part of the GEOTRACES program, which aims to document trace elements cycles in the ocean by a better understanding of their sources and sinks, including their export by particles (Henderson et al., 2007). Constraining the drivers of the particle-solution exchanges is thus an important issue in this area.

In this context, we present the first basin scale section of PREE concentrations and fractionation patterns in suspended particles collected in the Subpolar North Atlantic (SPNA), along the GEOVIDE section, from the surface to 1500 m depth. In the following, we specifically discuss processes affecting the PREE distribution such as lithogenic inputs from the margins, influence of biological activity and the role of ionic radius on their fate in the water column.

## 2 Methods

### 2.1 Study area: hydrographical and biogeochemical context

Samples were collected in the epipelagic and mesopelagic zones (0 m – 1500 m) during the GEOVIDE cruise (16th of May 2014 to 30th of June 2014, R/V Pourquoi Pas?) along the transect presented in Fig. 1. This figure also presents the main surface currents, as described in details in Zunino et al. (2017) and García-Ibáñez et al. (2018), together with the three main biogeochemical provinces identified by Longhurst (1995) and described in details by Lemaitre et al. (2018b): the subtropical North Atlantic (NAST), the North Atlantic drift (NADR) and the Arctic (ARCT) regions. The location of the stations where suspended particles were sampled (Fig. 1) were chosen to be representative of the diversity of water masses (Fig. 2) and biogeochemical provinces (Sarhou et al., 2018). Warm and salty waters coming from the tropical Atlantic are advected towards the Arctic by the North Atlantic Current (NAC, see Table 1 for abbreviation list). In response to air-sea exchanges and mixing with polar waters, surface waters become colder and fresher, but more importantly, denser. Thus, they tend to mix with underlying waters, particularly during convection events triggered by storms. In the Nordic Seas (between 65°N and 80°N), the water column can be ventilated down to the bottom, while convection never exceeds 2000 m in the subpolar gyre. The freshly formed deep water then returns southwards mainly through western boundary currents (Daniault et al., 2016; García-Ibáñez et al., 2015, 2018; Zunino et al., 2017).

At the south east end of the section, the North Atlantic subtropical (NAST) province is characterized by warm and salty waters (García-Ibáñez et al., 2018; Longhurst, 1995; Reygondeau et al., 2018; Zunino et al., 2017). This province is depleted in nutrients despite being under influence of continental inputs, and was sampled during the declining stage of the cyanobacteria bloom (Lemaitre et al., 2018b). Stations #1 and #13 were sampled in the NAST. The North Atlantic Drift region (NADR) is located between the NAST and the Reykjanes ridge, with higher nutrient concentrations than in the NAST (Longhurst, 1995).

100 A strong bloom of coccolithophorids, with a maximum intensity in the Icelandic basin, was occurring during the sampling time, and was associated with the highest primary production rate determined during the GEOVIDE cruise ( $1740 \text{ molC m}^{-2} \text{ d}^{-1}$ , station #26, Fonseca-Batista et al., 2019) and with high carbon export (up to  $80 \text{ molC m}^{-2} \text{ d}^{-1}$ , station #32, Lemaitre et al., 2018b). Four open ocean stations were sampled in this province: within the southern branch of the NAC (stations #21 and #32), at the Subpolar front (station #26) and above the Reykjanes Ridge (station #38).

105 West of the Reykjanes Ridge, the Irminger and Labrador Seas (Fig. 1) located in the Arctic region (ARCT) were nutrient-replete. Large blooms of diatoms occurred in this area, with a maximum of primary production at the end of May, three weeks before the GEOVIDE sampling in the Labrador Sea and one month before the sampling in the Irminger Sea (Lemaitre et al., 2018b). The western part of the ARCT region is under the influence of the Newfoundland margin. In this province, station #44 was sampled in the middle of the gyre, station #51 in the East Greenland Coastal Current (EGCC) and station #53 on the Greenland shelf. In the Labrador Sea, station #64 was influenced by the West Greenland Current (following the EGCC after it crossed Cape Farewell) while station #69 was located within the formation area of LSW, where strong convection events  
110 occurred the winter before GEOVIDE (García-Ibáñez et al., 2018; de Jong and de Steur, 2016). Westward, the station #77 was located close to the Newfoundland margin (ca 300 km).

## 2.2 Sampling at sea

Suspended particles were collected with 12 L Niskin bottles mounted on a standard rosette and samples were dedicated to the concentration analyses of particulate barium in excess ( $\text{Ba}_{\text{xs}}$ , biogenic Ba), dissolved and particulate REE (including Nd isotopic composition) and yttrium (often integrated to REE as chemical analogue, named YREE in such case) as well as ancillary parameter analyses, including particulate 232-thorium ( $^{232}\text{Th}$ ). The description of the sampling and filtration methods for water collected with this rosette follows that of Lemaitre et al. (2018b). Briefly, sampling was focused on the epipelagic (0 m – 200 m) and mesopelagic zones (200 m – 1500 m). Sampling bottles were shaken three times as recommended in the GEOTRACES cookbook (<https://geotracesold.sedoo.fr/Cookbook.pdf>), to avoid the loss of particles by sticking to the walls  
115 or settling at the bottom of the bottle. Then, four to eight liters of seawater were filtered off-line using clean slightly air pressurized containers (Perspex®). Suspended particles were collected onto polycarbonate filters of  $0.4 \mu\text{m}$  porosity (Nuclepore®, 47 mm or 90 mm of diameter). After sample filtration, the filter was rinsed with  $\leq 5 \text{ mL}$  of ultra-pure water (Milli-Q;  $18.2 \text{ M}\Omega \text{ cm}$ ) to remove most of sea salts. Finally, filters were carefully removed using plastic tweezers and were dried under a laminar flow hood at ambient temperature then stored in clean Petri dishes. Samples were handled in line in order  
120 to avoid contamination.

Ba,  $^{232}\text{Th}$ , yttrium Y and PREE digestion procedure were performed on the same sample and the resulting solution was shared between analysts.  $^{232}\text{Th}$  and Ba (but not Y) were first measured at the Royal Museum for Central Africa (Tervuren, Belgium), then Ba,  $^{232}\text{Th}$ , Y and PREE were later analyzed at LEGOS (Toulouse, France; this work). Details of this procedure are described in section 2.3.1.

130 A clean sampling system was also deployed at the same stations to collect suspended particles dedicated to the analysis of trace metals prone to contamination like iron (Fe) or zinc (Zn). It was composed of a clean rosette equipped with 12 L GO-FLO bottles. Suspended particulate samples were collected on paired polyethersulfone and mixed ester cellulose filters of 0.45  $\mu\text{m}$  and 5  $\mu\text{m}$  porosity, respectively. The sample digestion and the subsequent analytical work were conducted in LEMAR, Brest (Gourain et al., 2019). The digestion procedure was slightly different than the procedure used on filters collected with  
135 the standard rosette (see section 2.3.2). Ba and Y were also measured on these “clean samples” together with other trace metals, in Brest.

## 2.3 Sample preparation and analysis

### 2.3.1 Leaching procedure and analysis for the PYREE

Polycarbonate filters mounted on the Perspex® filtration units were first cut into two parts using a ceramic blade. One half  
140 was archived, while the other half was placed in a clean Teflon vial (Savillex®). The filter was then digested at Tervuren with a strong acid solution made of 1.5 mL HCl, 1 mL HNO<sub>3</sub> and 0.5 mL HF, all concentrated (Merck® Suprapur Grades) (Lemaitre et al., 2018b). Vials were left on hot plates at 90°C overnight. After this, the filter was fully digested, and the solution was then evaporated until near dryness. Finally, 13 mL of 0.32 mol L<sup>-1</sup> HNO<sub>3</sub> (Merck® Suprapur Grades) were added in the Savillex®  
145 vials and the leaching solutions were transferred into clean polypropylene tubes (VWR™). Then, Y, Ba, <sup>232</sup>Th and REE concentrations were measured using 2 mL of these archive solutions. Only few samples required an additional dilution by a factor between 1.3 and 1.5 using HNO<sub>3</sub> 0.32 mol L<sup>-1</sup> (prepared from Merck® nitric acid 65%, EMSURE® distilled twice at LEGOS to get the purest product), because the archive solution volume was below 2mL, which is the volume required by the ICP-MS measurement. These aliquots were placed in clean 5 mL polypropylene tubes and doped with a solution containing In and Re (ca. 100 ppt of both tracers) in order to correct matrix effects and sensitivity shifts during analysis. Analyses were  
150 performed at the Observatoire Midi Pyrénées (Toulouse, France) using a high-resolution inductively coupled plasma mass spectrometer (SF-ICP-MS, Element XR, Thermo Fischer Scientific®) in low resolution mode. The SF-ICP-MS was coupled to a desolvating nebulizer (Aridus II, CETAC Technologies®) to minimize oxide and hydroxide production rates and thus (hydr)oxide interferences (Aries et al., 2000). Oxide production rates were determined at the beginning and the end of every session using a Ce solution (CeO<0.03%). Other REE (hydr)oxides rates were then determined using the constant  
155 proportionality factor between them, previously determined with the same analytical configuration (Aries et al., 2000). Oxide-hydroxide interferences represented 0.001% to 1% of the signal except for Eu (0.3% to 10%). Isobaric interferences were corrected directly by the software of the ICP-MS, and thoroughly checked before the session. A five-point calibration curve was established using a multi elemental standard solution at the beginning, the middle and the end of the analysis. The 20.10<sup>-12</sup> g g<sup>-1</sup> of REE standard was measured every 5 samples. Standards were prepared by the dilution of a multi element stock  
160 solution (SCP Science, PlasmaCAL, Custom standard) in 0.32 mol L<sup>-1</sup> HNO<sub>3</sub> with ca 0.1 ppb of In and of Re, to match the relative concentrations measured in the samples. The certified reference material SLRS-5 (NRC Canada) was systematically

analyzed with the samples and their concentrations are within the error bar of the consensual values published by Yeghicheyan et al. (2013), with a smaller error (see Fig. S1). Reproducibility was assessed by measuring two or three times 2 mL of 23 samples from the same leaching solution. The difference between replicates varied from 0 % to 20%, and were mostly under 10%. The average percentage of difference between these analytical replicates is presented on Fig. S2. Procedural blanks have been estimated by conducting the same chemical procedure on clean, unused filters. The average chemical blank (n = 8) represented 0.01% to 5% of the sample concentrations, except for Y and Lu for which the contribution of the blank was generally higher (between 1% and 30%). Blanks were finally subtracted to the measured concentrations. Four sources of errors could affect the final data: errors on i) the proportion of filter analyzed that comes from cutting the filters in halves; ii) the volume of leachate; iii) the volume taken in the archive for analysis; iv) the standard deviation associated with ICP-MS measurements. The final error was calculated by propagating the uncertainties of these different sources, except for the cutting error, which is rather theoretical than empirical and was impossible to evaluate at the time. We assumed that particles had a homogenous distribution on the filters as heterogeneity is difficult to assess. This hypothesis is supported by the good agreement of Y, Ba and  $^{232}\text{Th}$  between the samples from Niskin bottles and the samples from GO-FLO bottles, which were not cut in halves (see section 2.3.2 below). The different errors, their method of calculation and their comparison are summarized in Fig. S3.

### 2.3.2 Laboratory to laboratory comparisons and validation of our data

Ba and  $^{232}\text{Th}$  results were used to compare the data obtained between Tervuren and Toulouse in order to assess the consistency of the different ICP-MS analyses. Y was used to compare the consistency of data obtained between Brest and Toulouse using two different sampling systems, filtration, digestion and analytical procedures. Y concentrations were more specifically used to validate the YREE sampling with the standard rosette, which is less prone to contamination than Fe or Zn, as underlined by van de Flierdt et al. (2012).

Results are presented in Fig. S4. Analytical determination of Ba and  $^{232}\text{Th}$  concentrations were performed in Toulouse and Tervuren (Lemaitre et al., 2018b). In Tervuren, an inductively coupled plasma quadrupole mass spectrometer (ICP-QMS; X Series 2 Thermo Fischer®) was used, while a high-resolution mass spectrometer was used in Toulouse (HR-ICP-MS; Element XR Thermo Fischer®). “Toulouse” vs. “Tervuren” Ba concentrations show a regression slope of 0.86 ( $r^2=0.91$ ,  $n=198$ ). For  $^{232}\text{Th}$ , “Toulouse” vs. “Tervuren” concentrations show a slope of 1.05 ( $r^2=0.98$ ,  $n=198$ ; Fig. S4).

The comparison between the two sampling and subsequent analytical procedures is illustrated by Y concentrations analyzed in “Brest” and “Toulouse”. In Brest, filters collected with the clean-rosette were leached with a mixture of HF and  $\text{HNO}_3$  during 4 hours at  $130^\circ\text{C}$  before evaporation (for details see Gourain et al., 2019), while in Toulouse, filters collected with the standard rosette were digested with a HCl, HF and  $\text{HNO}_3$  solution (see above section 2.3.1). The comparison shows an excellent consistency between both datasets: for Y, the regression slope is 0.93 ( $r^2=0.82$ ,  $n=78$ ; Figure S4). For Ba, the regression slope

is 0.86 ( $r^2=0.91$ ,  $n=78$ ). This intercomparison exercise supports the excellent reliability of our PREE data and allows us to discuss the PREE concentrations in the context of trace metal concentrations from Gourain et al. (2019) in the following parts.

### 195 3 Results

Concentrations of PY, PREE, PBa and  $P^{232}\text{Th}$  are compiled in Table 2. For sake of clarity, we only displayed PCe, PNd and PYb concentrations (Fig. 2 and 3) since these three REEs represent the light REE (Nd), heavy REE (Yb) and a specific behavior (Ce). Noteworthy, LREE and HREE are not equally influenced by dissolved-particulate exchanges (Koeppenkastrop et al., 1991; Koeppenkastrop and De Carlo, 1992, 1993; Sholkovitz, 1992; Sholkovitz et al., 1994). As free trivalent LREE are more abundant in seawater, they are more prone to adsorption on particles than HREE (Schijf et al., 2015). The specific behavior of Ce is due to the occurrence of its IV oxidation state in addition to the III oxidation state common to all the REE. Two mechanisms for Ce oxidation have been proposed so far: a microbially mediated oxidation in seawater under oxic conditions that leads to formation of insoluble  $\text{CeO}_2$ , more particle reactive than Ce(III) (Byrne and Kim, 1990; Elderfield, 1988; Moffett, 1990, 1994; Sholkovitz and Schneider, 1991) and an oxidative scavenging onto Mn oxides particles (De Carlo et al., 1997; Koeppenkastrop and De Carlo, 1992). These two processes act in addition to the general scavenging process that affects all the trivalent REE by surface complexation, thus leading to the Ce enrichment in particles and its stronger depletion in the dissolved phase compared to other REE.

Particulate Ce concentrations are higher than PNd concentrations (Fig. 2; Fig. 3 A and B), which are higher than PYb concentrations (Fig. 3 C and D), in agreement with the natural abundance and reactivity of these three REE: the light Ce and Nd are more abundant than the heavy Yb, and Ce is the most particle-reactive of the REE.

#### 3.1 Cerium

As shown in Fig. 2, particulate Ce concentrations varied between  $0.2 \text{ pmol L}^{-1}$  (station #64) and  $16.3 \text{ pmol L}^{-1}$  (station #32; Fig. 2). They were higher close to the Iberian margin (station #1:  $1 \text{ pmol L}^{-1} < \text{PCe} < 9.4 \text{ pmol L}^{-1}$ ) and on the Greenland shelf (station #53:  $5.7 \text{ pmol L}^{-1} < \text{PCe} < 14.6 \text{ pmol L}^{-1}$ ). In the NAST (station #13) and the NADR (stations #21 to #38) regions, vertical profiles presented a surface or subsurface maximum at all stations. A second maximum was observed at 160 m at station #13 and in the NADR region (except close to the subarctic front, at station #26). Below 200 m depth, PCe concentrations decreased and reached a value of  $2 \text{ pmol L}^{-1}$  within the mesopelagic area. Particulate Ce concentrations were higher to the east of the subarctic front (stations #13 and #21) compared to the west (stations #26, #32 and #38). In the ARCT region, surface PCe concentrations were lower and increased between 80 m and 160 m, with all  $\text{PCe} > 1 \text{ pmol L}^{-1}$  at all open-sea stations. Maximum concentrations were observed just below 200 m, at stations #44, #64 and #69. At depths greater than 200 m, PCe concentrations were more variable in the ARCT region than in the NADR region. They were higher than those observed at the surface except at station #69 where they remained between  $1 \text{ pmol L}^{-1}$  and  $2 \text{ pmol L}^{-1}$ . Particulate Ce profiles differed from that of PNd and PYb at two stations only: station #38, where higher concentrations were observed at 100 m and 800 m for PCe

only; station #44, where P<sub>Ce</sub> concentrations were more variable in the epipelagic zone than P<sub>Nd</sub> and P<sub>Yb</sub>, with maxima located at 120 m and 160 m depth. These maxima were not observed for other PREE at this station.

### 3.2 Neodymium

As for P<sub>Ce</sub> (and other PREE, see supplementary information and Table 2), P<sub>Nd</sub> concentrations were the highest close to the Iberian and Greenland margins with values up to 4.5 pmol L<sup>-1</sup> in the upper 100 m (Fig. 3 A and B). Concentrations decreased as the distance to margins increased, as seen at stations #13 where P<sub>Nd</sub> were lower than 1 pmol L<sup>-1</sup>. Low P<sub>Nd</sub> values were also measured at station #77, which is relatively close to the Newfoundland margin, yet located outside of the continental shelf.

### 3.3 Ytterbium

Distributions of P<sub>Nd</sub> and P<sub>Yb</sub> differed in several ways (Fig. 3). Stations #13, #44 and #69 displayed a maximum in subsurface for P<sub>Yb</sub> that was not observed for P<sub>Nd</sub>. In contrast, a local maximum in P<sub>Nd</sub> was identified at 160 m at stations #64 and #69, but not for P<sub>Yb</sub>. In the open ocean, at stations #21, #26, #32 and #38, concentrations of both elements were higher in the surface layer than below. The highest P<sub>Yb</sub> concentrations were determined in the NADR region, which was the most productive at the time of the cruise (Fonseca-Batista et al., 2019). Concentrations then decreased with depth to become constant, except at station #38 where they increased again in the mesopelagic zone (below 300 m). In the ARCT region, surface concentrations of P<sub>Nd</sub> were lower at 100 m than at 250 m, similar to station #1 contrasting on this point with the NADR region.

### 3.4 P<sub>Yb<sub>N</sub>}/P<sub>Nd<sub>N</sub></sub> ratios</sub>

To highlight a possible fractionation between LREE and HREE, the P<sub>Yb<sub>N</sub>}/P<sub>Nd<sub>N</sub></sub> ratio is calculated from concentrations normalized to the Post Archean Australian Shale (PAAS), commonly used for REE normalization, in order to get rid of the natural abundance “zig zag distribution” of the REE (Piper and Bau, 2013). This normalization allows i) a better diagnostic of the fractionation between PREE and ii) comparison with patterns in the literature. Results are presented in Fig. 4. The P<sub>Yb<sub>N</sub>}/P<sub>Nd<sub>N</sub></sub> ratio varied between 0.2 and 4.5, with an outlier (9) at station #13 at 40 m. Lower ratios (< 1) were observed along the margins, increasing with the distance from the coast. In the open ocean, except at station #38, P<sub>Yb<sub>N</sub>}/P<sub>Nd<sub>N</sub></sub> was higher at the surface (> 1.4), and decreased in the subsurface layers, ranging between 1 and 1.4. At station# 38, it was smaller than 1 in the upper 100 m and around 1 below. The lowest P<sub>Yb<sub>N</sub>}/P<sub>Nd<sub>N</sub></sub> ratio was determined in the core of the epipelagic zone at station #21 at 100 m (Fig. 4), where high concentrations of P<sub>La</sub>, P<sub>Ce</sub>, P<sub>Pr</sub> and P<sub>Nd</sub> (in other words, LREE) were measured. However, for other stations with a similar enrichment, no low P<sub>Yb<sub>N</sub>}/P<sub>Nd<sub>N</sub></sub> ratios were observed (stations #21 at 600m, #32 at 450 m and #38 at 800 m).</sub></sub></sub></sub></sub>



## 4 Discussion

### 4.1 Comparison with other studies

Particulate REE data in suspended particles are very scarce in the literature. To our knowledge, for the North Atlantic, only one other set of concentrations was published by Kuss et al. (2001), who measured PREE in samples centrifuged from several  
255 m<sup>3</sup> of water at a depth of 7 m, collected along the 20°W meridian between 30°N and 60°N. Even though this study is located in a different area of the North Atlantic Ocean, and only in surface, similarities can be pointed out. Kuss et al. (2001) observed PCE concentrations ranging between 0.2 pmol L<sup>-1</sup> and 4.9 pmol L<sup>-1</sup> with higher concentrations close to the margins especially near the Iberian margin, consistent with our data. Their PNd concentrations of ca. 0.5 pmol L<sup>-1</sup> to the south east of the NADR are also consistent with ours. The PNd concentrations reported by Tachikawa et al. (1999b) at a station located in a mesotrophic  
260 zone of the north-east tropical Atlantic and directly influenced by Saharan dust (6 g m<sup>-2</sup> yr<sup>-1</sup> to 15 g m<sup>-2</sup> yr<sup>-1</sup>, Rea, 1994) were almost 2 times higher than those reported here (PNd = 2.6 pmol L<sup>-1</sup> at 10 m at station M, when PNd <1.4 pmol L<sup>-1</sup> for GEOVIDE at 10 m; Fig. S5). The same authors measured lower concentrations than ours at the oligotrophic site of their study, where the dust flux was lower than at the mesotrophic site (4-5 g m<sup>-2</sup> yr<sup>-1</sup>, Rea, 1994) but higher than that found during the GEOVIDE cruise (2 ng m<sup>-3</sup> to 500 ng m<sup>-3</sup>, Shelley et al., 2017). Interestingly, PCE concentrations measured by these authors  
265 are similar to those reported in this study, for both the mesotrophic and oligotrophic sites. The difference of concentrations observed for the other PREE can be due to the fact that particle concentrations are usually higher in the subpolar North Atlantic than in the tropical Atlantic (Gehlen et al., 2006).

### 4.2 Lithogenic and authigenic PREE fractions

Particulate REE are found in both the lithogenic and authigenic phases of particles. Schematically, particles are often  
270 represented with a “lithogenic core” coated by authigenic material (Bayon et al., 2004; Sholkovitz et al., 1994). The “lithogenic core” has an external origin, product of the continental weathering transported by the winds or discharged by the rivers to the continental margins. The authigenic phases are produced in the water column, and particulate REE present in this phase can result from surface biological activity or scavenging by organic coatings and/or iron and manganese oxides and hydroxides (Bau, 1999; Bau and Koschinsky, 2009; Lam et al., 2015). Traces of the biological absorption can be found in inorganic  
275 planktonic tests (CaCO<sub>3</sub>, Palmer, 1985; Roberts et al., 2012 and BSi, Akagi, 2013) or in biogenic byproducts like barite (Ba<sub>xs</sub>, Garcia-Solsona et al., 2014; Guichard et al., 1979). The common view is that LREE are more sensitive to oxide phases of Fe and Mn, while HREE, more soluble, could preferentially react with biogenic phases (Akagi, 2013; Bertram and Elderfield, 1992; Grenier et al., 2018; Pham et al., 2019). In the Bering Strait, Akagi et al (2011) also observed a strong association between particulate HREE and biogenic silica collected in sediment traps. This specific BSi control on HREE behavior is  
280 discussed in section 4.6. Distribution coefficients also vary between HREE and LREE with depth and the nature of the particle phases (Schijf et al., 2015).

Thus, differentiating the distribution of REE [between the lithogenic and authigenic phases](#) can allow estimating the fraction implied in scavenging and/or absorption processes by the authigenic phase, while the lithogenic fraction can be used to picture continental inputs. The lithogenic REE fraction could also be estimated using conservative lithogenic tracers such as Al, <sup>232</sup>Th or Ti (e.g. Gourain et al., 2019; Tachikawa et al., 1997). These authors used Al as a lithogenic tracer while here we chose to use <sup>232</sup>Th. Indeed, the lithogenic fractions calculated from particulate Al (PAI) concentrations were often higher than 100% in surface waters close to the margins, revealing that a fraction of the total PAI is likely in the authigenic phase (Lerner et al., 2018; Van Beueskom et al., 1997). In addition, as Al is more prone to contamination, it was sampled with the clean rosette (Gourain et al., 2019), while <sup>232</sup>Th was measured in the same samples as PREE, collected with the standard rosette. The concentration of the lithogenic PREE fraction in particles is calculated by multiplying the <sup>232</sup>Th concentration in a given sample by the ratio of the considered REE on <sup>232</sup>Th in the upper continental crust (UCC, Rudnick and Gao, 2014, Eq. (1)), a value [similar to the uniform <sup>232</sup>Th concentrations reported by Chase et al. \(2001\) in marine sediments from cores of the South Atlantic.](#)

$$[RE]_{litho} = [^{232}Th] \times \left( \frac{[RE]}{[^{232}Th]} \right)_{UCC} \quad (1)$$

$$\%REE_{litho} = \frac{[RE]_{litho}}{[RE]} \times 100 \quad (2)$$

$$\%REE_{authi} = 100 - \%REE_{litho} \quad (3)$$

These PREE lithogenic concentrations are then divided by the total PREE concentrations to obtain the fraction of particulate REE of lithogenic origin (Eq. (2)). The authigenic fraction is then obtained by subtracting the lithogenic fraction from 100 % (Eq. (3)).

The percentage of lithogenic PNd along the section is represented in Fig. 5. In this figure, we also chose to represent the average value of the lithogenic fractions of the remaining PREE for the PLREE at five selected stations, excepted for PCe because of its distinctive behavior that leads to higher affinity for particles. We also plotted the PHREE at the same stations (#1, #26, #51, #53 and #77). Error bars represent the standard deviation of the resulting averages. These five stations are representative of the three dominant biogeochemical contexts observed along the section: [under lithogenic input influence \(#1, #53\), dominated by biological activity \(#26, #51\), and influenced by both \(#77\).](#) Sometimes, the estimated Nd lithogenic fraction exceeded 100% (up to 550% at 20m at station #1, and up to 130% at 160 m at station #13 and at 200 m at station #32). This suggests an excess of <sup>232</sup>Th in the particles, likely authigenic, or a difference between the adsorption kinetics of <sup>232</sup>Th and REE, as reported by Hayes et al. (2015). [In these cases, we capped the lithogenic proportion to 100%. The occurrence of an authigenic fraction of <sup>232</sup>Th may lead to a bias in the calculation of the lithogenic contribution and an overestimation of lithogenic contributions cannot be excluded at the surface. However, <sup>232</sup>Th remains predominantly lithogenic, and the comparison between the fractions calculated with Al and <sup>232</sup>Th provided in Fig. S6 for stations #1, #13, #32, #51 and #77 validates the use of <sup>232</sup>Th](#)

### 4.3 PAAS normalization and REE patterns

The patterns of PAAS-normalized concentrations are represented in Fig. 5 together with the profiles for the same five stations as in 4.2. For ease of reading, patterns are averaged by depth intervals displaying similar values. Error bars represent the standard deviation of the concentration series. A dissolved REE pattern obtained in the North Atlantic Deep Water at 12°S at 2499 m (Zheng et al., 2016) is also represented, for comparison with a “typical” dissolved seawater pattern, marked by a negative Ce anomaly and a pronounced normalized HREE/LREE positive slope (De Baar et al., 1985; Elderfield, 1988; Elderfield and Greaves, 1982; Tachikawa et al., 1999a). The patterns of other stations are represented in Fig. S7.

The validity of using PAAS for normalization is assessed by the fact that PAAS does not present any significant difference in REE composition between shales and loess from Europe, North America and China (Rudnick and Gao, 2014), that are potential sources of lithogenic material for Europe and North America. The flat patterns obtained at stations #1, #13 and #53 validate a PAAS-like source of lithogenic material. Normalization to atmospheric depositions has been put aside as these inputs were very low during the cruise (Shelley et al., 2017), and the REE patterns of these dusts are not available. In addition, normalization to dusts would not have allowed us to compare our data with the REE patterns in the literature, which commonly uses PAAS to normalize.

### 4.4 Lithogenic supply at the margins

The high PREE concentrations close to the Iberian margin and on the Greenland shelf suggest that particulate material is released by the margins to the water column (Fig. 3 and Table 2), the highest concentrations being measured at station #1 (Fig. 5). At these stations, the lithogenic PREE fractions range between 50% and 100% (Fig. 3). The relatively flat total PREE patterns displayed at these stations show only a slight enrichment in LREE due to their preferential scavenging compared to the HREE (Fig. 5; Sholkovitz et al., 1994).

High percentages of lithogenic PREE were visible along two isopycnals ( $\sigma_0=27.05$  and  $\sigma_0=27.4$ ) visible from station #1 to station #32 (in other words beyond the Subpolar Front) spreading over 1700 km from the Iberian margin (Fig. 6). Similar maxima have been reported for lithogenic particulate iron (PFe) and particulate manganese (PMn) by Gourain et al., 2019 (their Fig. 6 B).

Above the Greenland shelf, at station #53, the fraction of lithogenic PREE was also high (55% to 86% for PNd), only slightly lower than at station #1, with a median lithogenic contribution of 59% for PLREE and 83% for PHREE (Fig. 5). Unlike what was observed to the south eastern end of GEOVIDE section from station #1 to #26, these lithogenic particles do not spread offshore. Indeed, except at the surface, the lithogenic fraction for LREE was lower than 50% at stations #51 and #64 in the Irminger Sea and in the Labrador Sea, respectively. This can be explained by the circulation: the East Greenland Irminger Current (EGIC) is a strong narrow current bypassing Greenland along its shelf ( $23.4 \pm 1.9$  Sv, Daniault et al., 2016), likely

preventing exchanges between the Irminger Subpolar Mode Water (IrSBPMW) and waters of the Greenland shelf, transported by the EGCC current which flows parallel to the coast (green and orange arrows around the Greenland southeastern tip in Fig. 1). Our observations are consistent with those of Lacan and Jeandel (2005), who showed that the Nd isotopic signatures ( $\epsilon_{Nd}$ ) of SPMW transported by the EGIC do not vary significantly along the Greenland shelf. In the same way, the lithogenic influence is moderate at station #77, where land-ocean exchanges are reduced due to the EGCC ( $1.5 \pm 0.2$  Sv, Daniault et al., 2016). While the lithogenic fraction is still relatively high at this station ( $50\% < REE_{litho} < 80\%$  below 150m), the fractionated patterns indicate that other processes are at play (Fig. 5), like for example preferential scavenging of LREE on Mn and Fe oxyhydroxides (Bau, 1999) and/or fractionation by diatoms (Akagi et al., 2011). The roughly constant lithogenic contribution around 60% at station #77 indicates that like around Greenland, no nepheloid layers are spreading from the Newfoundland margin, at least at the time of the cruise.

Gourain et al. (2019) reported similar results for lithogenic PFe and PMn fractions estimated during the same cruise. These authors also observed a strong contribution of lithogenic material from the Iberian margin spreading until station #32, a lower contribution along the Newfoundland margin and almost no lithogenic contribution from the slope of the Greenland margin. Using lithogenic PMn as a tracer of sediment resuspension, they estimated that 100% of PMn was originating from sediment resuspension at station #1 between 250 m and 1000 m (their Fig. 4). Interestingly, E. Le Roy (Le Roy, 2019) observed an unexpected maximum of  $^{227}Ac$  activity at 500 m at stations #1 and #21, indicating the influence of a sediment source, also consistent with the PREE lithogenic fraction. However, at station #13, the lithogenic PREE maximum was not found at the same depth as for  $^{227}Ac$  (160 m instead of 200m). Unfortunately, the different sampling resolutions for PREE and  $^{227}Ac$  did not permit to further compare data between these tracers except at the surface of station #1, where a maximum of  $^{227}Ac$  was consistent with the lithogenic PREE signal.

These highly enriched depths in lithogenic tracers could be due to the formation of intermediate nepheloid layers (INL) at 250 m and 500 m along the Iberian margin, similar to those revealed slightly more north by McCave and Hall (2002). A contribution of the Mediterranean Water (MW) to these high concentrations and lithogenic proportions cannot be excluded, but the lack of data in the core of the MW (1000 m to 1500 m, García-Ibáñez et al., 2018) prevented us to conclude further.

A highly energetic process is needed to generate strong resuspension of lithogenic matter. It may result from the friction and energetic excitation of internal waves along the continental slope (Cacchione, 2002). Another possible source is the erosion of the coast by the strong current (from  $0.05 \text{ m s}^{-1}$  to  $0.1 \text{ m s}^{-1}$ ) coming out from Gibraltar and flowing northward along the Iberian margin (Gourain et al., 2019; McCave and Hall, 2002; Zunino et al., 2017). A combination of all these dynamic processes, generating internal waves south of station #1 could have led to strong sediment resuspension, and subsequent advection of resulting particles northward by the current.

To sum up, margins can provide significant amounts of particulate lithogenic REE to the ocean that must be considered in the mass balance of REE. Occurrence and magnitude of these inputs depend on the morphology of the margin, the hydrodynamical forcing and the amount and composition of sediments leading (or not) to the formation of nepheloid layers.

#### 4.5 Rare Earth Element fractionation: Ce anomalies

380 As briefly mentioned above, Ce presents a unique chemistry among REE elements with the coexistence of a trivalent and a  
tetravalent form. In seawater, the redox cycle of Ce and Mn are strongly linked (Bau and Dulski, 1996; Elderfield, 1988;  
Moffett, 1990, 1994). Biotic and abiotic oxidations of Ce have been previously reported. In seawater, the oxidation of  $Ce^{3+}$  in  
385  $CeO_2$  is microbially catalyzed and the resulting tetravalent  $CeO_2$  is insoluble, and thus preferentially adsorbed by surface  
complexes of particles (Byrne and Kim, 1990; Elderfield, 1988; Moffett, 1990, 1994). This pattern of oxidation, which is  
similar to Mn oxidation, suggests a common mechanism and possible coprecipitation, yet with different kinetics (Moffett,  
1990, 1994). Mn oxides can catalyze Ce abiotic oxidation at the surface of particles, leading to an oxidative scavenging of Ce  
by Mn oxides (Bau, 1999; Bau and Koschinsky, 2009; Byrne and Kim, 1990; De Carlo et al., 1997; Koeppenkastrop and De  
Carlo, 1992). Also, a Ce enrichment in Fe hydroxides by sequential leaching of ferromanganese crusts has also been reported  
(Bau and Koschinsky, 2009). In contrast, experiments of REE addition during Mn oxide and Fe hydroxide precipitation showed  
390 little (Davranche et al., 2004) or no evidence of a preferential Ce scavenging by Fe hydroxides unlike for Mn oxides (De Carlo  
et al., 1997; Koeppenkastrop and De Carlo, 1992; Ohta and Kawabe, 2001). Therefore, the preferential Ce scavenging onto Fe  
hydroxides is still under debate. This exceptional behavior among REE results in a Ce depletion in seawater.

Conversely, in particles, this leads to a “symmetrical” Ce enrichment compared to other REE when concentrations are  
normalized to a lithogenic reference as PAAS (Garcia-Solsona et al., 2014; Tachikawa et al., 1999a). This Ce enrichment is  
395 quantified using the Ce anomaly, calculated with the concentrations normalized to PAAS. The expression of Bolhar et al.  
(2004, Eq. 4) is used in this paper:

$$\frac{Ce}{Ce^*} = \frac{[Ce]}{2 * [Pr] - [Nd]} \quad (4)$$

This expression uses Pr and Nd concentrations and is preferred to the one using La and Nd concentrations, as La can also  
400 present anomalies in seawater (Bau and Dulski, 1996).

In this dataset, most of Ce/Ce\* ratios are greater than one (i.e. positive anomaly). At stations #26, #32, #51 and #77 between  
the surface and ca. 100 m, PCe was depleted compared to other PREE, and  $(Ce/Ce^*) < 1$ . This surface minimum was followed  
by a pronounced positive anomaly down to 200 m. At deeper depths, the anomaly was relatively higher in the NADR region  
compared to the NAST and ARCT regions, where they are around 1 when they are  $\geq 1.2$  in the NADR region (Fig. 7).

405 In the NADR, between the surface and 50 m (stations #26 and #32) and between 20 m and 60 m (station #38, which showed  
a surprising positive anomaly at the surface), the negative PCe anomaly was related to the seawater-like patterns, produced by  
REE uptake in seawater during formation of biogenic matter (Garcia-Solsona et al., 2014; Tachikawa et al., 1999b): all REEs  
were absorbed from seawater without fractionation. These PCe anomalies were rather constant or showed a slight increase  
with depth until 50 m or 100 m, depending on the stations. Below, the PCe anomalies increased with depth. These PCe anomaly  
410 variations were consistent with the high productivity and export characterizing this area (Lemaitre et al., 2018b). Indeed, if  
particles were removed faster than Ce is oxidized, the Ce anomaly would have been limited with depth (Moffett, 1990). Two

factors could explain the step in Ce/Ce\* observed between 50 m and 100 m in the NADR: the beginning of remineralization in favor of the release of trivalent REE; and/or a decrease of the particle settling speed, in favor of CeO<sub>2</sub> adsorption from seawater and precipitation of Mn oxides which catalyzed Ce oxidation onto particles. Both factors could act simultaneously.

415 The anomaly became even larger between 200 m and 400 m depending on the profiles, and was constant below 600 m, suggesting an equilibrium between Ce oxidation, trivalent REE desorption and remineralization processes. The behavior of P<sub>Ce</sub> at station #21 was less clear, the profile displaying strong vertical variations (Fig. 7B): an important increase in Ce/Ce\* was observed at 40 m depth, then Ce/Ce\* decreased at 200m to a value similar to the surface one. These sharp variations suggested an influence of lithogenic particles, which was not observed at the other stations. A comparison between P<sub>Ce</sub>

420 lithogenic fractions and of the Ce anomaly vertical profiles showed mirror variations: less pronounced P<sub>Ce</sub> anomalies were correlated to higher P<sub>Ce</sub> lithogenic proportions (Fig. S8). This could be explained by advection of quite well preserved lithogenic material with smooth Ce anomaly. This is consistent with the spreading of nepheloid layers from the Iberian margin discussed above.

In the ARCT region, negative anomalies were also determined at the surface, but they were less pronounced than in the NADR region (Fig. 7). The P<sub>Ce</sub> anomalies increased down to 200 m at stations #44, #51, #64 and #77 but remained lower than in the NADR region for the same depth range. These profiles could be compared to the profiles of stations #26 and #32, with a rather constant P<sub>Ce</sub> anomaly in the first meters that increased after a “critical” depth (here about 40 m versus 100 m in the NADR). The P<sub>Ce</sub> anomaly was then roughly constant below 200 m at stations #51, #64 and #69. At stations #44 and #77, the anomaly increased below 700 m and 1000 m, respectively. The weaker negative anomaly at the surface was consistent with a lower

430 primary production (Lemaitre et al., 2018b). The roughly constant P<sub>Ce</sub> anomaly at depths below 200m indicated that equilibrium between biotic and abiotic Ce oxidation, adsorption and remineralization of trivalent REE was reached faster in the ARCT region.

At station #69, high P<sub>Ce</sub> positive anomalies were observed at the surface and there was no significant increase of the anomaly with depth. These variations were consistent with the fraction of lithogenic P<sub>Ce</sub> but not as much as at station #21, where the

435 lithogenic fraction was smaller (<60 %, Fig. S8). At this station, the equilibrium between the reactions leading to a P<sub>Ce</sub> enrichment and adsorption-remineralization of all REE was reached at ca. 100 m, which was deeper than at the other stations of the region, suggesting a lower particle flux. At station #53, Ce anomaly was roughly constant (around 1), which is consistent with a station dominated by lithogenic inputs.

Four points displayed a Ce /Ce\*>3 (station #32 at 140 m and 450 m, station #38 at 100 m and station #64 at 140 m). Although

440 we cannot exclude punctual contamination in Ce during the sampling, we do not have a clear explanation and decided not to consider these data further. They are reported under brackets in Table 2 and not included in the figures.

#### **4.6 The influence of biological activity on the PREE distributions**

At stations #26, #32, #38 and #44 which displayed a seawater-like pattern at the surface, the formation of biogenic matter associated with high particle fluxes could explain the negative Ce anomaly and high PY<sub>bN</sub>/PN<sub>dN</sub> ratios (>1 and up to 4.5).

445 These patterns were progressively attenuating with depth due to the Ce oxidation discussed in the preceding section. However, the enrichment in HREE could reach 1000 m (Fig. 4), while the negative Ce anomaly was never observed at depths deeper than 100 m. Yet surprising, this could indicate that HREE are not fully associated with the soft tissues of the biogenic material. A LREE enrichment was simultaneously observed, consistent with the preferential scavenging of LREE onto solid phases.

When looking more closely to the authigenic phase of these samples, an uncommon enrichment of PHREE was observed, 450 consistent with the total PREE patterns (Fig. 5 and S7). A strong primary production was determined at all these stations (Fonseca-Batista et al., 2019), so the preferential transfer of HREE from the dissolved phase to the authigenic particulate phase likely occurred when the biological stripping was active. This transfer seemed to have been even more important in the ARCT region, leading to more pronounced HREE enrichments, while the strongest bloom was observed in the NADR region. In the ARCT surface waters the  $PYb_N/PNd_N$  could reach 4.5, whereas  $PYb_N/PNd_N$  never exceeded 3 in the NADR region. In the 455 ARCT region, the bloom was dominated by diatoms, still active at station #51 and #44, and declining at the others (Fonseca-Batista et al., 2019; Lemaitre et al., 2018b). This declining bloom led to a strong export, but high remineralization rates decreased the biological imprint in favor of the lithogenic signature at depth (Fig. 5). Thus, we suspect that biological uptake had a strong effect on the total and authigenic PREE patterns observed during GEOVIDE. A relationship between HREE and biogenic silica (BSi) was suggested by Akagi (2013), following thermodynamic calculations. According to this work, between 460 40% and 65% of REE form a  $REE(H_3SiO_4)^{2+}$  could complex with silicic acid in the deep North Atlantic. Complexation of REE with silicates was further confirmed by Patten and Byrne (2017), although these authors estimated a lower complexation constant, and a smaller fraction of silica-complexed REE. In addition, significant correlations were observed between dissolved Si and dissolved HREE by Bertram and Elderfield (1992; western Indian Ocean), Stichel et al. (2012) and Garcia-Solsona et al. (2014, both in the Atlantic sector of Southern Ocean), Grenier et al. (2018; Kerguelen Islands) and Pham et al. (2019; 465 Solomon Sea). Contrastingly, in other areas, Patten and Byrne (laboratory experiment, 2017, their Fig.7) and Zheng et al. (tropical South Atlantic, 2016, their Fig. 11) showed that the relationship between  $SiOH_4$  and REE was either curvilinear or not significant. In our study, the highest surface authigenic  $PYb_N/PNd_N$  ratios were located in the Irminger and Labrador Seas, where the highest BSi concentrations of the GEOVIDE section were also measured (Sarhou et al., 2018) (Fig. S9A and B). A correlation between BSi and PHREE concentrations was detected although it remained weak, the highest correlation coefficient 470 being  $R^2=0.4$  for Lu. Interestingly, this correlation coefficient increased with the atomic mass number, confirming that BSi has a significant effect on authigenic PHREE distributions, from Tb to Lu, but not on lighter REE (Fig. S9 C). These correlations may indicate that in some areas characterized by high diatom blooms, the HREE distributions could be partly linked to the BSi formation, in agreement with Akagi's hypotheses. This relationship would depend on the abundance and the nature of particles (i.e. the occurrence of diatoms), and on the speciation of REE in the dissolved phase (de Baar et al., 2018). Akagi, (2013) 475 suggested that silica-REEs complexes could be incorporated during frustule formation, but the mechanism underlying this enrichment during diatom blooms still has to be clarified. Linking it to what is known about complexation and adsorption processes of the REE is beyond the scope of this work. In addition, an effective relationship between BSi and PHREE can be

blurred by other scavenging processes involving particulate Mn and Fe (hydr)oxides, also known to influence the slope between LREE and HREE.

480 If diatoms are effectively preferentially incorporating the HREE, the high prevalence of coccolithophorids characterizing the NADR bloom (Lemaitre et al., 2018b) could explain the relatively low HREE enrichment in surface. Besides, patterns flatten with depth to present a quasi-lithogenic signature below 60 m, suggesting that particles with a strong organic signature did not reach this depth at the time of sampling.

#### 4.7 The PAAS-normalized particulate Ho/Y ratio: a proxy of processes independent of the ionic radius

485 Yttrium (Y) and the lanthanide holmium (Ho) are characterized by roughly the same ionic radius and charge, making them “geochemical twins” (Bau, 1999). The PAAS-normalized particulate ratio ( $PHo_N/PY_N$ ) highlights differences in their distributions, and therefore allows identifying radius-independent fractionation processes affecting YREE in seawater. We choose to normalize  $PHo/PY$  measured in our particulate samples to the PAAS ratio in order to reveal any relative loss or enrichment compared to continental material (Fig. 8). Because of different electron configurations, Ho is more prone to  
490 establish ionic bounds, and thus to be preferentially adsorbed onto (hydr)oxides like  $FeOH_3$  and  $MnO_2$ . In comparison, Y preferentially establishes covalent bounds, and will be preferentially absorbed compared to Ho (Censi et al., 2007; Bau, 1999; Bau et al., 1995). Along the GEOVIDE section,  $PHo_N/PY_N$  ratio varied between 0.4 and 1.5, with most of the values being smaller than 1 (i.e. depleted in Ho compared to PAAS). To assess the influence of  $FeOH_3$  and  $MnO_2$  on  $PHo_N/PY_N$  distributions, we calculated their concentrations using the formula of Lam et al. (2015) and  $PMn$  and  $PFe$  data from Gourain  
495 et al. (2019). There was no obvious relationship between  $PHo_N/PY_N$  and  $FeOH_3$  and  $MnO_2$  (Fig. 9). Noteworthy,  $PHo_N/PY_N$  ratios were higher when  $[Fe(OH)_3] > 10^{-2} \mu g L^{-1}$  and when  $MnO_2$  content increased. However, the  $PHo_N/PY_N$  ratio was low ( $<0.6$ ) in the Labrador Sea surface waters (station #69), the Irminger Sea (stations #44 and #51) and from the surface to 750 m depth in the NADR region (stations #21, #26 and #32; Fig. 8). This is consistent with the fact that both these locations are depleted in  $MnO_2$  and  $Fe(OH)_3$ , leading to a weak adsorption of Ho (Fig. 9). All along the section, low  $PHo_N/PY_N$  ratios were  
500 observed from the surface to 800 m depth at productive stations (stations #21, #26 and #32,  $PHo_N/PY_N < 0.9$ ). This suggested a preferential absorption of Y during the formation of biogenic matter, as reported by Censi et al. (2007). In the NADR region, between 200 m and 600 m depth,  $PCe$  anomalies were positive ( $>1$ ), PHREE were enriched, and  $PHo$  concentrations were relatively depleted at stations #26 and #21 ( $PHo_N/PY_N < 1$ ). The low remineralization rates observed in this area (Lemaitre et al., 2018a) could explain the enrichment of  $PY$  concentrations at the surface. At Station # 32, high  $PHo$  concentrations between  
505 350 m and 600 m depth was concomitant with the largest  $PCe$  positive anomaly ( $>1.2$ ), indicating intensive adsorption processes, leading to an enhanced scavenging of REE.

In the ARCT region, at station #69, slightly lower  $PHo_N/PY_N$  ratios were observed compared to the other stations of this region (0.5 at the surface, around 0.7 to 0.9 with depth). This station was characterized by a low primary production and the highest remineralization rates of the section (Fonseca-Batista et al., 2019; Lemaitre et al., 2018b, 2018a). This could have led to high



510 adsorption of Ho relative to Y. As Ho is more prone to be released from particles than Y, a lower  $\text{PHo}_\text{N}/\text{PY}_\text{N}$  ratio was observed. The higher  $\text{PHo}_\text{N}/\text{PY}_\text{N}$  ratios determined at the other ARCT stations point to scavenging by particles, although the Ce anomaly was lower than in the NADR region.

Although the  $\text{PHo}_\text{N}/\text{PY}_\text{N}$  ratios were not directly correlated to  $\text{MnO}_2$  and  $\text{Fe}(\text{OH})_3$  estimated concentrations, this ratio was lower when the primary production was high, in agreement with a preferential incorporation of Y into the biogenic matter. The change of  $\text{PHo}_\text{N}/\text{PY}_\text{N}$  ratios with depth reflects a balance between two processes: the preferential scavenging of Ho by adsorption onto  $\text{MnO}_2$  (identified with P Ce anomalies) and remineralization.

## 5 Conclusion

Particulate concentrations of the fourteen Rare Earth Elements and  $^{232}\text{Th}$  have been measured in 200 samples of suspended particles collected in the epipelagic and mesopelagic zones of the Subpolar North Atlantic during the GEOVIDE cruise (GEOTRACES GA01) during late spring - early summer of 2014, providing one of the only available PREE distribution snapshots in the North Atlantic. All PREE concentrations were higher close to the margins (stations #1 and #51), especially at the Iberian margin and on the Greenland shelf (station #53). These high concentrations contrasted with the low concentrations measured in the surface waters of the NADR region (stations #26, #32 and #38) and in the Irminger Sea (station #44).

The use of  $^{232}\text{Th}$  as a lithogenic tracer allowed identifying the lithogenic and authigenic REE fractions. The greatest PREE lithogenic fractions were determined close to the Iberian margin, where 80 % to 100% of PREE have a lithogenic origin, in particular within two nepheloid layers located at 250 m and 500 m depth. These two nepheloid layers extended westward, mostly along isopycnals  $\sigma_0=27.05$  and  $\sigma_0=27.4$ . This lithogenic signature was still visible at station #32, in other words at 1700 km from the margin, due to strong currents and energetic dynamics potentially enhanced by internal waves. Lower lithogenic fractions, between 50 and 80% of REE, were determined close to the Newfoundland margin, and on the Greenland shelf (station #53). No significant lithogenic inputs could be observed far from the Greenland shelf at stations #51 and #64. This is due to the strong EGIC current that prevents exchanges between the shelf and the open ocean.

The influence of biological activity on REE scavenging has also been evaluated. In areas of high biological productivity, the authigenic phase of particles was enriched in HREE compared to LREE. These particles also displayed negative P Ce anomalies, as well as low  $\text{PHo}_\text{N}/\text{Y}_\text{N}$  ratios, suggesting recently formed particles with a preferential uptake of HREE and Y by absorption. In the NADR region, P Ce anomaly and LREE enrichment increased with depth, while  $\text{PHo}_\text{N}/\text{PY}_\text{N}$  ratio remained low ( $<1$ ). Low remineralization rates could maintain low  $\text{PHo}_\text{N}/\text{PY}_\text{N}$  ratios while promoting exchanges with the dissolved phase. This also led to the building of the P Ce anomaly through sorption processes and to PLREE enrichment. In the Labrador Sea, remineralization rates were higher, moderate P Ce positive anomalies were observed together with low  $\text{PHo}_\text{N}/\text{PY}_\text{N}$  ratios ( $1 < \text{P Ce}/\text{Ce}^* < 1.2$ ,  $\text{PHo}_\text{N}/\text{PY}_\text{N} < 1$ ). High remineralization rates could have induced an increase in exchanges between particulate and the dissolved pools, leading to a lower number of adsorption sites on the authigenic coatings, and to subsequent lower P Ce anomalies. The low  $\text{PHo}_\text{N}/\text{PY}_\text{N}$  ratios can also be attributed to these reduced exchanges. Thus, our results suggested

that the  $\text{PHo}_N/\text{PY}_N$  ratios were less controlled by  $\text{MnO}_2$  and  $\text{Fe}(\text{OH})_3$  than previously proposed but more likely controlled by other processes such as absorption and adsorption that do not involve these two (hydr)oxides.

We also highlighted the importance of biogenic silica on HREE preferential scavenging, shown by a clear increase of the PHREE concentrations in the surface waters of the ARCT region, where a massive diatom bloom occurred. The correlation coefficient between BSi and REE concentrations showed no particular links with the atomic mass number from La to Gd, while it increased from Tb to Lu. This relationship was only observed for PHREE and the underlying mechanisms will have to be investigated in future studies.

## 550 **Acknowledgments**

We deeply thank the crew of the N/O Pourquoi Pas? whose implication was invaluable during the cruise. Geraldine Sarthou, PI of GEOVIDE with Pascale Lherminier (co-author) is acknowledged for her serene management of this long cruise. We also thank Emmanuel de Saint-Léger and Fabien Perault from the DT INSU for their precious technical help all along the cruise.

We thank Aurelie Marquet, Camille Duquenoy and Jerome Chmeleff for making the (sometimes capricious) HR-ICP-MS operational. Many thanks to Michael Bau for the fruitful discussion we had during the Goldschmidt conference. This work was supported by the French National Research Agency (ANR-13-BS06-0014, ANR-12-PDOC-0025-01), the French National Centre for Scientific Research (CNRS-LEFECYBER, UMR 5566). The logistics were supported by DT-INSU and GENAVIR.

We also deeply acknowledge Rob Sherrell and one anonymous reviewer whose comments helped us to improve this manuscript.

## 560 **References**

- Akagi, T.: Rare earth element (REE)–silicic acid complexes in seawater to explain the incorporation of REEs in opal and the “leftover” REEs in surface water: New interpretation of dissolved REE distribution profiles, *Geochimica et Cosmochimica Acta*, 113, 174–192, doi:10.1016/j.gca.2013.03.014, 2013.
- Akagi, T., Fu, F., Hongo, Y. and Takahashi, K.: Composition of rare earth elements in settling particles collected in the highly productive North Pacific Ocean and Bering Sea: Implications for siliceous-matter dissolution kinetics and formation of two REE-enriched phases, *Geochimica et Cosmochimica Acta*, 75(17), 4857–4876, doi:10.1016/j.gca.2011.06.001, 2011.
- Aries, S., Valladon, M., Polvé, M. and Dupré, B.: A Routine Method for Oxide and Hydroxide Interference Corrections in ICP-MS Chemical Analysis of Environmental and Geological Samples, *Geostandards and Geoanalytical Research*, 24(1), 19–31, doi:10.1111/j.1751-908X.2000.tb00583.x, 2000.
- de Baar, H. J. W., Bruland, K. W., Schijf, J., van Heuven, S. M. A. C. and Behrens, M. K.: Low cerium among the dissolved rare earth elements in the central North Pacific Ocean, *Geochimica et Cosmochimica Acta*, 236, 5–40, doi:10.1016/j.gca.2018.03.003, 2018.
- Bau, M.: Scavenging of dissolved yttrium and rare earths by precipitating iron oxyhydroxide: Experimental evidence for Ce oxidation, Y-Ho fractionation, and lanthanide tetrad effect, *Geochim. Cosmochim. Ac.*, 63(1), 67–77, 1999.

- 575 Bau, M. and Dulski, P.: Distribution of yttrium and rare-earth elements in the Penge and Kuruman iron-formations, Transvaal Supergroup, South Africa, *Precambrian Research*, 79(1–2), 37–55, doi:10.1016/0301-9268(95)00087-9, 1996.
- Bau, M. and Koschinsky, A.: Oxidative scavenging of cerium on hydrous Fe oxide: Evidence from the distribution of rare earth elements and yttrium between Fe oxides and Mn oxides in hydrogenetic ferromanganese crusts, *Geochem. J.*, 43(1), 37–47, doi:10.2343/geochemj.1.0005, 2009.
- 580 Bayon, G., German, C. R., Burton, K. W., Nesbitt, R. W. and Rogers, N.: Sedimentary Fe–Mn oxyhydroxides as paleoceanographic archives and the role of aeolian flux in regulating oceanic dissolved REE, *Earth and Planetary Science Letters*, 224(3–4), 477–492, doi:10.1016/j.epsl.2004.05.033, 2004.
- Bertram, C.J. and Elderfield, H.: The geochemical balance of the rare earth elements and neodymium isotopes in the oceans, *Geochim. Cosmochim. Ac.*, 57, 1957–1986, 1992.
- 585 Bolhar, R., Kamber, B. S., Moorbath, S., Fedo, C. M. and Whitehouse, M. J.: Characterisation of early Archaean chemical sediments by trace element signatures, *Earth and Planetary Science Letters*, 222(1), 43–60, doi:10.1016/j.epsl.2004.02.016, 2004.
- Byrne, R. H. and Kim, K.-H.: Rare earth element scavenging in seawater, *Geochimica et Cosmochimica Acta*, 54(10), 2645–2656, doi:10.1016/0016-7037(90)90002-3, 1990.
- 590 Cacchione, D. A.: The Shaping of Continental Slopes by Internal Tides, *Science*, 296(5568), 724–727, doi:10.1126/science.1069803, 2002.
- Censi, P., Zuddas, P., Larocca, D., Saiano, F., Placenti, F. and Bonanno, A.: Recognition of water masses according to geochemical signatures in the Central Mediterranean sea: Y/Ho ratio and rare earth element behaviour, *Chemistry and Ecology*, 23(2), 139–153, doi:10.1080/02757540701197879, 2007.
- 595 Chase, Z., Anderson, R. F. and Fleisher, M. Q.: Evidence from authigenic uranium for increased productivity of the glacial subantarctic ocean, *Paleoceanography*, 16(5), 468–478, doi:10.1029/2000PA000542, 2001.
- Crecelius, E. A.: The solubility of coal fly ash and marine aerosols in seawater, *Marine Chemistry*, 8(3), 245–250, doi:10.1016/0304-4203(80)90013-4, 1980.
- Daniault, N., Mercier, H., Lherminier, P., Sarafanov, A., Falina, A., Zunino, P., Pérez, F. F., Ríos, A. F., Ferron, B., Huck, T.,
- 600 Thierry, V. and Gladyshev, S.: The northern North Atlantic Ocean mean circulation in the early 21st century, *Progress in Oceanography*, 146, 142–158, doi:10.1016/j.pocean.2016.06.007, 2016.
- Davranche, M., Pourret, O., Gruau, G. and Dia, A.: Impact of humate complexation on the adsorption of REE onto Fe oxyhydroxide, *Journal of Colloid and Interface Science*, 277(2), 271–279, doi:10.1016/j.jcis.2004.04.007, 2004.
- De Baar, H. J. W., Bacon, M. P., Brewer, P. G. and Bruland, K. W.: Rare earth elements in the Pacific and Atlantic Oceans, *Geochimica et Cosmochimica Acta*, 49(9), 1943–1959, doi:10.1016/0016-7037(85)90089-4, 1985.
- 605 De Carlo, E. H., Wen, X.-Y. and Irving, M.: The Influence of Redox Reactions on the Uptake of Dissolved Ce by Suspended Fe and Mn Oxide Particles, *Aquatic Geochemistry*, 3(4), 357–389, doi:10.1023/A:1009664626181, 1997.

- Elderfield, H.: The oceanic chemistry of the rare-earth elements, *Philosophical Transactions of the Royal Society of London*, A(325), 105–126, 1988.
- 610 Elderfield, H. and Greaves, M. J.: The rare earth elements in seawater, *Nature*, 296(5854), 214–219, doi:10.1038/296214a0, 1982.
- van de Fliedert, T., Pahnke, K., Amakawa, H., Andersson, P., Basak, C., Coles, B., Colin, C., Crocket, K., Frank, M., Frank, N., Goldstein, S. L., Goswami, V., Haley, B. A., Hathorne, E. C., Hemming, S. R., Henderson, G. M., Jeandel, C., Jones, K., Kreissig, K., Lacan, F., Lambelet, M., Martin, E. E., Newkirk, D. R., Obata, H., Pena, L., Piotrowski, A. M., Pradoux, C.,
- 615 Scher, H. D., Schöberg, H., Singh, S. K., Stichel, T., Tazoe, H., Vance, D. and Yang, J.: GEOTRACES intercalibration of neodymium isotopes and rare earth element concentrations in seawater and suspended particles. Part 1: reproducibility of results for the international intercomparison: Intercalibration of Seawater Nd Isotopes, *Limnol. Oceanogr. Methods*, 10(4), 234–251, doi:10.4319/lom.2012.10.234, 2012.
- Fonseca-Batista, D., Li, X., Riou, V., Michotey, V., Deman, F., Fripiat, F., Guasco, S., Brion, N., Lemaitre, N., Tonnard, M.,
- 620 Gallinari, M., Planquette, H., Planchon, F., Sarthou, G., Elskens, M., LaRoche, J., Chou, L. and Dehairs, F.: Evidence of high N<sub>2</sub> fixation rates in the temperate northeast Atlantic, *Biogeosciences*, 16(5), 999–1017, doi:10.5194/bg-16-999-2019, 2019.
- Fowler, S. W. and Knauer, G. A.: Role of large particles in the transport of elements and organic compounds through the oceanic water column, *Progress in Oceanography*, 16(3), 147–194, doi:10.1016/0079-6611(86)90032-7, 1986.
- García-Ibáñez, M. I., Pardo, P. C., Carracedo, L. I., Mercier, H., Lherminier, P., Ríos, A. F. and Pérez, F. F.: Structure,
- 625 transports and transformations of the water masses in the Atlantic Subpolar Gyre, *Progress in Oceanography*, 135, 18–36, doi:10.1016/j.pocean.2015.03.009, 2015.
- García-Ibáñez, M. I., Pérez, F. F., Lherminier, P., Zunino, P., Mercier, H. and Tréguer, P.: Water mass distributions and transports for the 2014 GEOVIDE cruise in the North Atlantic, *Biogeosciences*, 15(7), 2075–2090, doi:10.5194/bg-15-2075-2018, 2018.
- 630 Garcia-Solsona, E., Jeandel, C., Labatut, M., Lacan, F., Vance, D., Chavagnac, V. and Pradoux, C.: Rare earth elements and Nd isotopes tracing water mass mixing and particle-seawater interactions in the SE Atlantic, *Geochim. Cosmochim. Ac.*, 125, 351–372, 2014.
- Gehlen, M., Bopp, L., Emprin, N., Aumont, O., Heinze, C. and Ragueneau, O.: Reconciling surface ocean productivity, export fluxes and sediment composition in a global biogeochemical ocean model, 17, 2006.
- 635 Gourain, A., Planquette, H., Cheize, M., Lemaitre, N., Menzel Barraqueta, J.-L., Shelley, R., Lherminier, P. and Sarthou, G.: Inputs and processes affecting the distribution of particulate iron in the North Atlantic along the GEOVIDE (GEOTRACES GA01) section, *Biogeosciences*, 16(7), 1563–1582, doi:10.5194/bg-16-1563-2019, 2019.
- Grenier, M.: Differentiating Lithogenic Supplies, Water Mass Transport, and Biological Processes On and Off the Kerguelen Plateau Using Rare Earth Element Concentrations and Neodymium Isotopic Compositions, *Frontiers in Marine Science*, 5, 30,
- 640 2018.

- Guichard, F., Church, T. M., Treuil, M. and Jaffrezic, H.: Rare earths in barites: distribution and effects on aqueous partitioning, *Geochimica et Cosmochimica Acta*, 43(7), 983–997, doi:10.1016/0016-7037(79)90088-7, 1979.
- Hayes, C. T., Anderson, R. F., Fleisher, M. Q., Vivancos, S. M., Lam, P. J., Ohnemus, D. C., Huang, K.-F., Robinson, L. F., Lu, Y., Cheng, H., Edwards, R. L. and Moran, S. B.: Intensity of Th and Pa scavenging partitioned by particle chemistry in the North Atlantic Ocean, *Marine Chemistry*, 170, 49–60, doi:10.1016/j.marchem.2015.01.006, 2015.
- Henderson, G. M., Anderson, R. F., Adkins, J., Andersson, P., Boyle, E. A., Cutter, G., de Baar, H., Eisenhauer, A., Frank, M., Francois, R., Orians, K., Gamo, T., German, C., Jenkins, W., Moffett, J., Jeandel, C., Jickells, T., Krishnaswami, S., Mackey, D., Measures, C. I., Moore, J. K., Oeschies, A., Pollard, R., van der Loeff, M. R., Schlitzer, R., Sharma, M., von Damm, K., Zhang, J., Masque, P. and Grp, S. W.: GEOTRACES - An international study of the global marine biogeochemical cycles of trace elements and their isotopes, *CHEMIE DER ERDE-GEOCHEMISTRY*, 67(2), 85–131, doi:10.1016/j.chemer.2007.02.001, 2007.
- Jeandel, C. and Oelkers, E. H.: The influence of terrigenous particulate material dissolution on ocean chemistry and global element cycles, *Chemical Geology*, 395, 50–66, doi:10.1016/j.chemgeo.2014.12.001, 2015.
- Jeandel, C., Bishop, J. K. and Zindler, A.: Exchange of neodymium and its isotopes between seawater and small and large particles in the Sargasso Sea, *Geochimica et Cosmochimica Acta*, 59(3), 535–547, doi:10.1016/0016-7037(94)00367-U, 1995.
- Jeandel, C., Rutgers van der Loeff, M., Lam, P. J., Roy-Barman, M., Sherrell, R. M., Kretschmer, S., German, C. and Dehairs, F.: What did we learn about ocean particle dynamics in the GEOSECS–JGOFS era?, *Progress in Oceanography*, 133, 6–16, doi:10.1016/j.pocean.2014.12.018, 2015.
- de Jong, M. F. and de Steur, L.: Strong winter cooling over the Irminger Sea in winter 2014–2015, exceptional deep convection, and the emergence of anomalously low SST: Irminger sea cooling and convection, *Geophys. Res. Lett.*, 43(13), 7106–7113, doi:10.1002/2016GL069596, 2016.
- Khatiwala, S., Tanhua, T., Mikaloff Fletcher, S., Gerber, M., Doney, S. C., Graven, H. D., Gruber, N., McKinley, G. A., Murata, A., Ríos, A. F. and Sabine, C. L.: Global ocean storage of anthropogenic carbon, *Biogeosciences*, 10(4), 2169–2191, doi:10.5194/bg-10-2169-2013, 2013.
- Koepfenkastro, D. and De Carlo, E. H.: Sorption of rare-earth elements from seawater onto synthetic mineral particles: An experimental approach, *Chemical Geology*, 95(3), 251–263, doi:https://doi.org/10.1016/0009-2541(92)90015-W, 1992.
- Koepfenkastro, D. and De Carlo, E. H.: Uptake of rare earth elements from solution by metal oxides, *Environ. Sci. Technol.*, 27(9), 1796–1802, doi:10.1021/es00046a006, 1993.
- Koepfenkastro, D., De Carlo, E. H. and Roth, M.: A method to investigate the interaction of rare earth elements in aqueous solution with metal oxides, *Journal of Radioanalytical and Nuclear Chemistry*, 152(2), 337–346, doi:10.1007/BF02104687, 1991.
- Kuss, J., Garbe-Schönberg, C.-D. and Kremling, K.: Rare earth elements in suspended particulate material of North Atlantic surface waters, *Geochimica et Cosmochimica Acta*, 65(2), 187–199, doi:10.1016/S0016-7037(00)00518-4, 2001.

- 675 Kwon, E. Y., Primeau, F. and Sarmiento, J. L.: The impact of remineralization depth on the air–sea carbon balance, *Nature Geoscience*, 2(9), 630–635, doi:10.1038/ngeo612, 2009.
- Lacan, F. and Jeandel, C.: Acquisition of the neodymium isotopic composition of the North Atlantic Deep Water: neodymium isotopic composition, *Geochemistry, Geophysics, Geosystems*, 6(12), n/a-n/a, doi:10.1029/2005GC000956, 2005.
- Lam, P. J. and Marchal, O.: Insights into Particle Cycling from Thorium and Particle Data, *Annual Review of Marine Science*, 7(1), 159–184, doi:10.1146/annurev-marine-010814-015623, 2015.
- 680 Lam, P. J., Twining, B. S., Jeandel, C., Roychoudhury, A., Resing, J. A., Santschi, P. H. and Anderson, R. F.: Methods for analyzing the concentration and speciation of major and trace elements in marine particles, *Progress in Oceanography*, 133, 32–42, doi:10.1016/j.pocean.2015.01.005, 2015.
- Le Roy, E.: Distribution des radionucléides naturels ( $^{226}\text{Ra}$  et  $^{227}\text{Ac}$ ) le long de la section GA01 dans l’Atlantique Nord., Université de Toulouse III – Paul Sabatier, Toulouse. [online] Available from: <https://hal.archives-ouvertes.fr/tel-02454460>  
685 (Accessed 5 May 2020), 2019.
- Lemaitre, N., Planchon, F., Planquette, H., Dehairs, F., Fonseca-Batista, D., Roukaerts, A., Deman, F., Tang, Y., Mariez, C. and Sarthou, G.: High variability of particulate organic carbon export along the North Atlantic GEOTRACES section GA01 as deduced from  $^{234}\text{Th}$  fluxes, *Biogeosciences*, 15(21), 6417–6437, doi:10.5194/bg-15-6417-2018, 2018a.
- Lemaitre, N., Planquette, H., Sarthou, G., Jacquet, S., García-Ibáñez, M. I., Gourain, A., Cheize, M., Monin, L., André, L.,  
690 Laha, P., Terryn, H., Dehairs, F. and Dehairs, F.: Particulate barium tracing of significant mesopelagic carbon remineralisation in the North Atlantic, *Biogeosciences*, 15(8), 2289–2307, doi:10.5194/bg-15-2289-2018, 2018b.
- Lerner, P., Marchal, O., Lam, P. J. and Solow, A.: Effects of particle composition on thorium scavenging in the North Atlantic, *Geochimica et Cosmochimica Acta*, 233, 115–134, doi:10.1016/j.gca.2018.04.035, 2018.
- Lherminier, P. and Sarthou, G.: The 2014 Greenland-Portugal GEOVIDE CTDO2 hydrographic and SADCP data (GO-SHIP  
695 A25 and GEOTRACES GA01), SEANOE, doi:<https://doi.org/10.17882/52153>, 2017.
- Longhurst, A.: Seasonal cycles of pelagic production and consumption, *Progress in Oceanography*, 36(2), 77–167, doi:10.1016/0079-6611(95)00015-1, 1995.
- McCave, I. . and Hall, I. .: Turbidity of waters over the Northwest Iberian continental margin, *Progress in Oceanography*, 52(2–4), 299–313, doi:10.1016/S0079-6611(02)00012-5, 2002.
- 700 Menzel Barraqueta, J.-L., Schlosser, C., Planquette, H., Gourain, A., Cheize, M., Boutorh, J., Shelley, R., Contreira Pereira, L., Gledhill, M., Hopwood, M. J., Lacan, F., Lherminier, P., Sarthou, G. and Achterberg, E. P.: Aluminium in the North Atlantic Ocean and the Labrador Sea (GEOTRACES GA01 section): roles of continental inputs and biogenic particle removal, *Biogeosciences*, 15(16), 5271–5286, doi:10.5194/bg-15-5271-2018, 2018.
- Moffett, J. W.: Microbially mediated cerium oxidation in sea water, *Nature*, 345(6274), 421–423, doi:10.1038/345421a0, 1990.
- 705 Moffett, J. W.: The relationship between cerium and manganese oxidation in the marine environment, *Limnol. Oceanogr.*, 39(6), 1309–1318, doi:10.4319/lo.1994.39.6.1309, 1994.

- Ohnemus, D. C. and Lam, P. J.: Cycling of lithogenic marine particles in the US GEOTRACES North Atlantic transect, *Deep Sea Research Part II: Topical Studies in Oceanography*, 116, 283–302, doi:10.1016/j.dsr2.2014.11.019, 2015.
- Ohta, A. and Kawabe, I.: REE(III) adsorption onto Mn dioxide ( $\delta$ -MnO<sub>2</sub>) and Fe oxyhydroxide: Ce(III) oxidation by  $\delta$ -MnO<sub>2</sub>, *710 Geochimica and Cosmochimica Acta*, 65(5), 695–703, 2001.
- Palmer, M. R.: Rare earth elements in foraminifera tests, *Earth and Planetary Science Letters*, 73, 285–298, 1985.
- Pham, V. Q., Grenier, M., Cravatte, S., Michael, S., Jacquet, S., Belhadj, M., Nachez, Y., Germineaud, C. and Jeandel, C.: Dissolved rare earth elements distribution in the Solomon Sea, *Chemical Geology*, 524, 11–36, doi:10.1016/j.chemgeo.2019.05.012, 2019.
- 715 Phoebe J. Lam, Jong-Mi Lee, Maija I. Heller, Sanjin Mehic, Yang Xiang and Nicholas R. Bates: Size-fractionated distributions of suspended particle concentration and major phase composition from the U.S. GEOTRACES Eastern Pacific Zonal Transect (GP16), *Mar. Chem.*, doi:http://dx.doi.org/10.1016/j.marchem.2017.08.013, 2017.
- Piper, D. Z. and Bau, M.: Normalized Rare Earth Elements in Water, Sediments, and Wine: Identifying Sources and Environmental Redox Conditions, *AJAC*, 04(10), 69–83, doi:10.4236/ajac.2013.410A1009, 2013.
- 720 Planquette, H. and Sherrell, R. M.: Sampling for particulate trace element determination using water sampling bottles: methodology and comparison to in situ pumps, *Limnology and Oceanography: Methods*, 10(5), 367–388, doi:10.4319/lom.2012.10.367, 2012.
- R, S.: Ocean Data View, [online] Available from: <http://odv.awi.de>, 2016.
- Rea, D. K.: The paleoclimatic record provided by eolian deposition in the deep sea: The geologic history of wind, *725 Geophys.*, 32(2), 159, doi:10.1029/93RG03257, 1994.
- Reygondeau, G., Guidi, L., Beaugrand, G., Henson, S. A., Koubbi, P., MacKenzie, B. R., Sutton, T. T., Fioroni, M. and Maury, O.: Global biogeochemical provinces of the mesopelagic zone, *Journal of Biogeography*, 45(2), 500–514, doi:10.1111/jbi.13149, 2018.
- Roberts, N. L., Piotrowski, A. M., Elderfield, H., Eglinton, T. I. and Lomas, M. W.: Rare earth element association with  
730 foraminifera, *Geochimica et Cosmochimica Acta*, 94, 57–71, doi:10.1016/j.gca.2012.07.009, 2012.
- Rudnick, R. L. and Gao, S.: Composition of the Continental Crust, in *Treatise on Geochemistry*, pp. 1–51, Elsevier., 2014.
- Sanders, R., Henson, S. A., Koski, M., De La Rocha, C. L., Painter, S. C., Poulton, A. J., Riley, J., Salihoglu, B., Visser, A., Yool, A., Bellerby, R. and Martin, A. P.: The Biological Carbon Pump in the North Atlantic, *Progress in Oceanography*, 129, 200–218, doi:10.1016/j.pocean.2014.05.005, 2014.
- 735 Sarthou, G., Lherminier, P., Achterberg, E. P., Alonso-Pérez, F., Bucciarelli, E., Boutorh, J., Bouvier, V., Boyle, E. A., Branellac, P., Carracedo, L. I., Casacuberta, N., Castrillejo, M., Cheize, M., Contreira Pereira, L., Cossa, D., Daniault, N., De Saint-Léger, E., Dehairs, F., Deng, F., Desprez de Gésincourt, F., Devesa, J., Foliot, L., Fonseca-Batista, D., Gallinari, M., García-Ibáñez, M. I., Gourain, A., Grossteffan, E., Hamon, M., Heimbürger, L. E., Henderson, G. M., Jeandel, C., Kermabon, C., Lacan, F., Le Bot, P., Le Goff, M., Le Roy, E., Lefèbvre, A., Leizour, S., Lemaitre, N., Masqué, P., Ménage, O., Menzel  
740 Barraqueta, J.-L., Mercier, H., Perault, F., Pérez, F. F., Planquette, H. F., Planchon, F., Roukaerts, A., Sanial, V., Sauzède, R.,

- Schmechtig, C., Shelley, R. U., Stewart, G., Sutton, J. N., Tang, Y., Tisnérat-Laborde, N., Tonnard, M., Tréguer, P., van Beek, P., Zurbrick, C. M. and Zunino, P.: Introduction to the French GEOTRACES North Atlantic Transect (GA01): GEOVIDE cruise, *Biogeosciences*, 15(23), 7097–7109, doi:10.5194/bg-15-7097-2018, 2018.
- Schijf, J., Christenson, E. A. and Byrne, R. H.: YREE scavenging in seawater: A new look at an old model, *Marine Chemistry*, 177, 460–471, doi:10.1016/j.marchem.2015.06.010, 2015.
- Shelley, R. U., Roca-Martí, M., Castrillejo, M., Sanial, V., Masqué, P., Landing, W. M., Beek, P. van, Planquette, H. and Sarthou, G.: Quantification of trace element atmospheric deposition fluxes to the Atlantic Ocean (>40°N; GEOVIDE, GEOTRACES GA01) during spring 2014, *Deep Sea Research Part I: Oceanographic Research Papers*, 119, 34–49, doi:https://doi.org/10.1016/j.dsr.2016.11.010, 2017.
- Sholkovitz, E. R.: Chemical evolution of rare earth elements: fractionation between colloidal and solution phases of filtered river water, *Earth and Planetary Science Letters*, 114(1), 77–84, doi:10.1016/0012-821X(92)90152-L, 1992.
- Sholkovitz, E. R. and Schneider, D. L.: Cerium redox cycles and rare earth elements in the Sargasso Sea, *Geochimica et Cosmochimica Acta*, 55(10), 2737–2743, doi:10.1016/0016-7037(91)90440-G, 1991.
- Sholkovitz, E. R., Landing, W. M. and Lewis, B. L.: Ocean particle chemistry: The fractionation of rare earth elements between suspended particles and seawater, *Geochimica et Cosmochimica Acta*, 58(6), 1567–1579, doi:10.1016/0016-7037(94)90559-2, 1994.
- Stemmann, L., Gorsky, G., Marty, J.-C., Picheral, M. and Miquel, J.-C.: Four-year study of large-particle vertical distribution (0–1000m) in the NW Mediterranean in relation to hydrology, phytoplankton, and vertical flux, *Deep Sea Research Part II: Topical Studies in Oceanography*, 49(11), 2143–2162, doi:10.1016/S0967-0645(02)00032-2, 2002.
- Tachikawa, K., Handel, C. and Dupré, B.: Distribution of rare earth elements and neodymium isotopes in settling particulate material of the tropical Atlantic Ocean (EUMELI site), *Deep Sea Research Part I: Oceanographic Research Papers*, 44(11), 1769–1792, doi:10.1016/S0967-0637(97)00057-5, 1997.
- Tachikawa, K., Jeandel, C. and Roy-Barman, M.: A new approach to the Nd residence time in the ocean: the role of atmospheric inputs, *Earth and Planetary Science Letters*, 170(4), 433–446, doi:10.1016/S0012-821X(99)00127-2, 1999a.
- Tachikawa, K., Jeandel, C., Vangriesheim, A. and Dupré, B.: Distribution of rare earth elements and neodymium isotopes in suspended particles of the tropical Atlantic Ocean (EUMELI site), *Deep Sea Research Part I: Oceanographic Research Papers*, 46(5), 733–755, doi:10.1016/S0967-0637(98)00089-2, 1999b.
- Tonnard, M., Planquette, H., Bowie, A. R., van der Merwe, P., Gallinari, M., Desprez de Gésincourt, F., Germain, Y., Gourain, A., Benetti, M., Reverdin, G., Tréguer, P., Boutorh, J., Cheize, M., Menzel Barraqueta, J.-L., Pereira-Contreira, L., Shelley, R., Lherminier, P. and Sarthou, G.: Dissolved iron in the North Atlantic Ocean and Labrador Sea along the GEOVIDE section (GEOTRACES section GA01), *Biogeosciences Discussions*, 1–53, doi:10.5194/bg-2018-147, 2018.
- Trull, T. W. and Armand, L.: Insights into Southern Ocean carbon export from the C of particles and dissolved inorganic carbon during the SOIREE iron release experiment, 26, 2001.



- 775 Turekian, K. K.: The fate of metals in the oceans, *Geochimica et Cosmochimica Acta*, 41(8), 1139–1144, doi:[https://doi-org-s.docadis.ups-tlse.fr/10.1016/0016-7037\(77\)90109-0](https://doi-org-s.docadis.ups-tlse.fr/10.1016/0016-7037(77)90109-0), 1977.
- Van Beueskom, J. E. E., Van Bennekom, A. J., Tréguer, P. and Morvan, J.: Aluminium and silicic acid in water and sediments of the Enderby and Crozet Basins, *Deep Sea Research Part II: Topical Studies in Oceanography*, 44(5), 987–1003, doi:[10.1016/S0967-0645\(96\)00105-1](https://doi.org/10.1016/S0967-0645(96)00105-1), 1997.
- 780 Yeghicheyan, D., Bossy, C., Bouhnik Le Coz, M., Douchet, C., Granier, G., Heimbürger, A., Lacan, F., Lanzaova, A., Rousseau, T. C. C., Seidel, J.-L., Tharaud, M., Candaudap, F., Chmeleff, J., Cloquet, C., Delpoux, S., Labatut, M., Losno, R., Pradoux, C., Sivry, Y. and Sonke, J. E.: A Compilation of Silicon, Rare Earth Element and Twenty-One other Trace Element Concentrations in the Natural River Water Reference Material SLRS-5 (NRC-CNRC), *Geostandards and Geoanalytical Research*, 37(4), 449–467, doi:[10.1111/j.1751-908X.2013.00232.x](https://doi.org/10.1111/j.1751-908X.2013.00232.x), 2013.
- 785 Zheng, X.-Y., Plancherel, Y., Saito, M. A., Scott, P. M. and Henderson, G. M.: Rare earth elements (REEs) in the tropical South Atlantic and quantitative deconvolution of their non-conservative behavior, *Geochimica et Cosmochimica Acta*, 177, 217–237, doi:[10.1016/j.gca.2016.01.018](https://doi.org/10.1016/j.gca.2016.01.018), 2016.
- Zunino, P., Lherminier, P., Mercier, H., Daniault, N., García-Ibáñez, M. I. and Pérez, F. F.: The GEOVIDE cruise in May–June 2014 reveals an intense Meridional Overturning Circulation over a cold and fresh subpolar North Atlantic, *Biogeosciences*, 14(23), 5323–5342, doi:[10.5194/bg-14-5323-2017](https://doi.org/10.5194/bg-14-5323-2017), 2017.

790

795

800

805

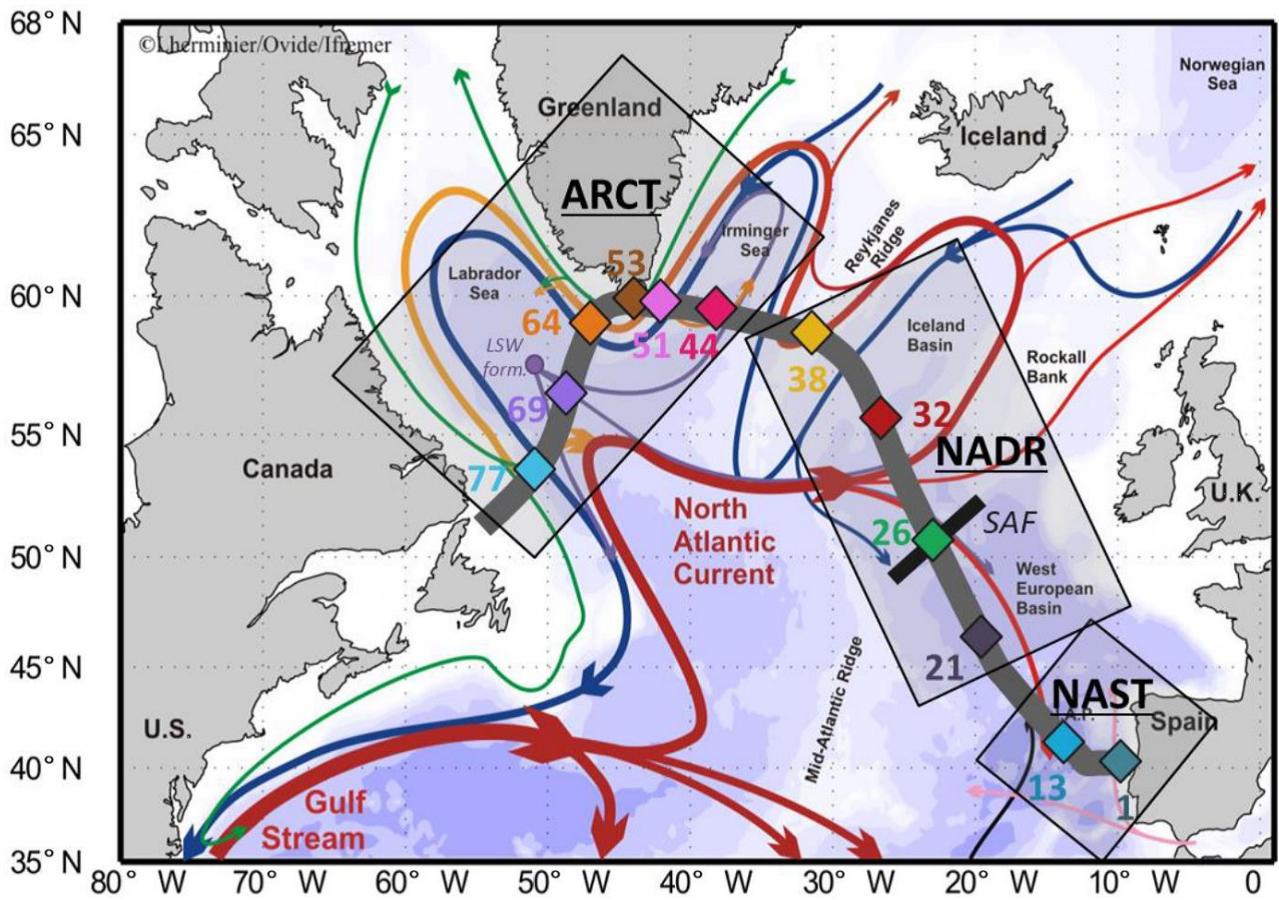
**Table 1: List of regions and water masses with their acronyms investigated in this study.**

<b>Regions</b>	
<b>SPNA</b>	Subpolar North Atlantic
<b>NAST</b>	North Atlantic Subtropical
<b>NADR</b>	North Atlantic drift
<b>ARCT</b>	Arctic
<b>Water masses</b>	
<b>ENACW</b>	East North Atlantic Central Water
<b>MW</b>	Mediterranean Water
<b>SAIW</b>	Subarctic Intermediate Water
<b>SPMW</b>	Subpolar Mode Water
<b>IrSPMW</b>	Irminger Subpolar Mode Water
<b>LSW</b>	Labrador Sea Water
<b>Currents</b>	
<b>NAC</b>	North Atlantic Current
<b>ERRC</b>	East Reykjanes Ridge Current
<b>IC</b>	Irminger Current
<b>EGIC</b>	East Greenland Irminger Current
<b>EGCC</b>	East Greenland Coastal Current

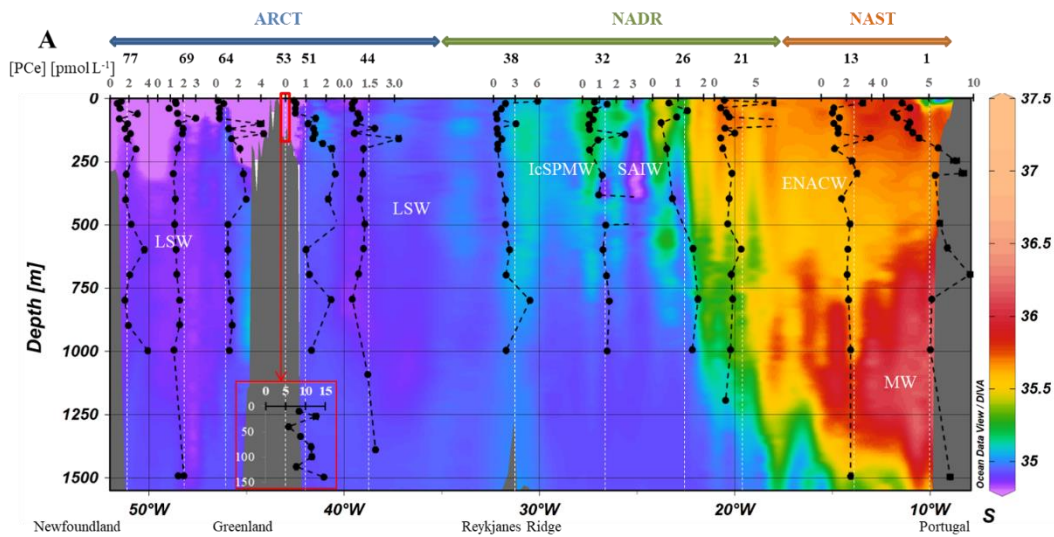




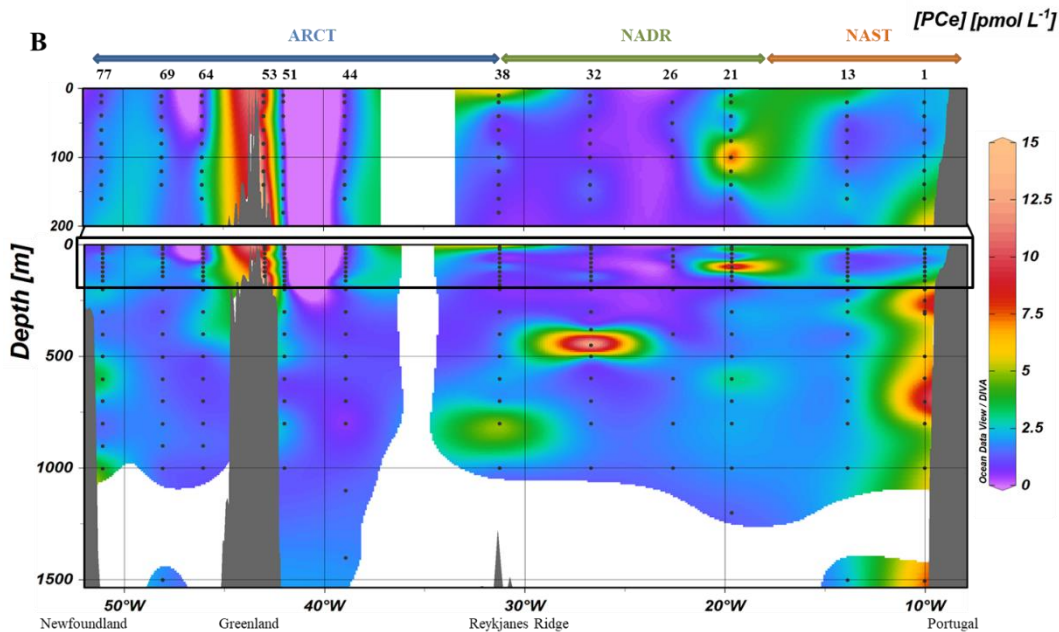




830 Figure 1: Map of the studied area (Subpolar North Atlantic, SPNA), including schematized circulation features, adapted from García-Ibáñez et al. (2015). Bathymetry is plotted in color with interval boundaries at 100 m, at 1000 m, and every 1000 m below 1000 m. Red and green arrows represent the main surface currents; pink and orange arrows represent currents at intermediate depths; blue and purple arrows represent the deep currents. Diamonds indicate station locations, in 3 distinct areas (grey squares): the North Atlantic Subtropical province (NAST), the North Atlantic Drift region (NADR), and the Arctic region (ARCT). The approximate locations of the subarctic front (SAF; black bar crossing station #26) and the formation site of the Labrador Sea Water (LSW form.) are also indicated. The section used in ODV figures is symbolized by the thick grey line. From (Lemaitre et al., 2018b).



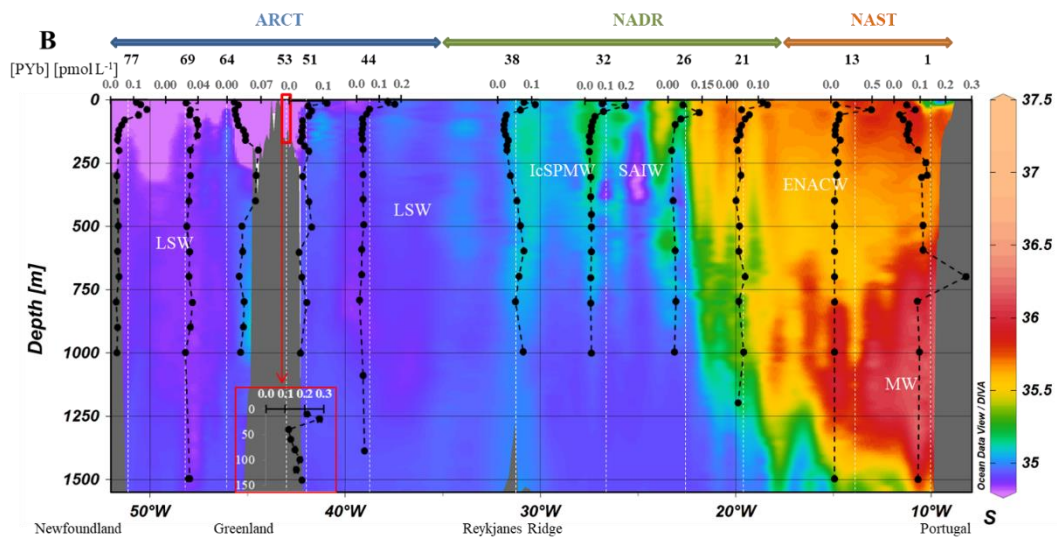
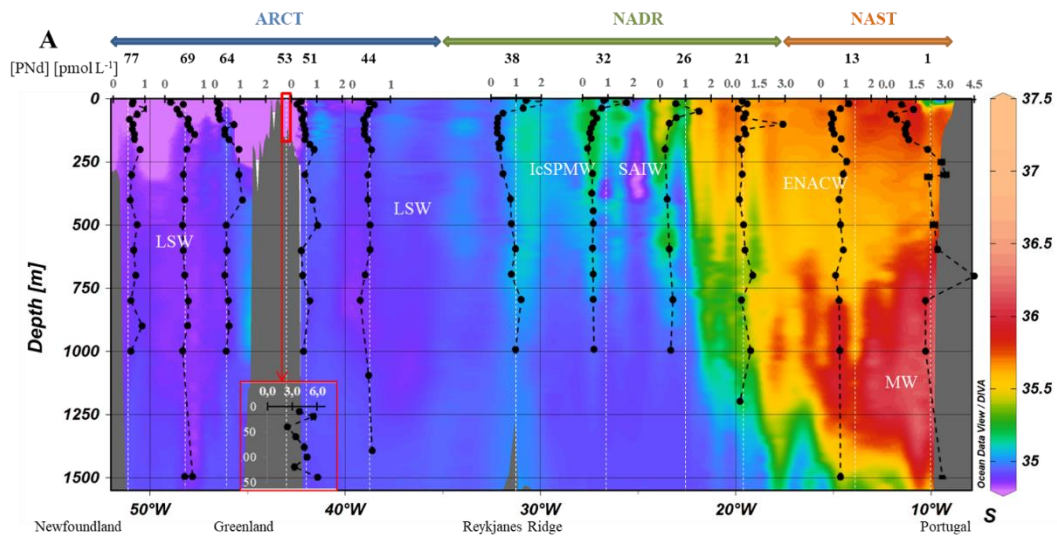
835



840

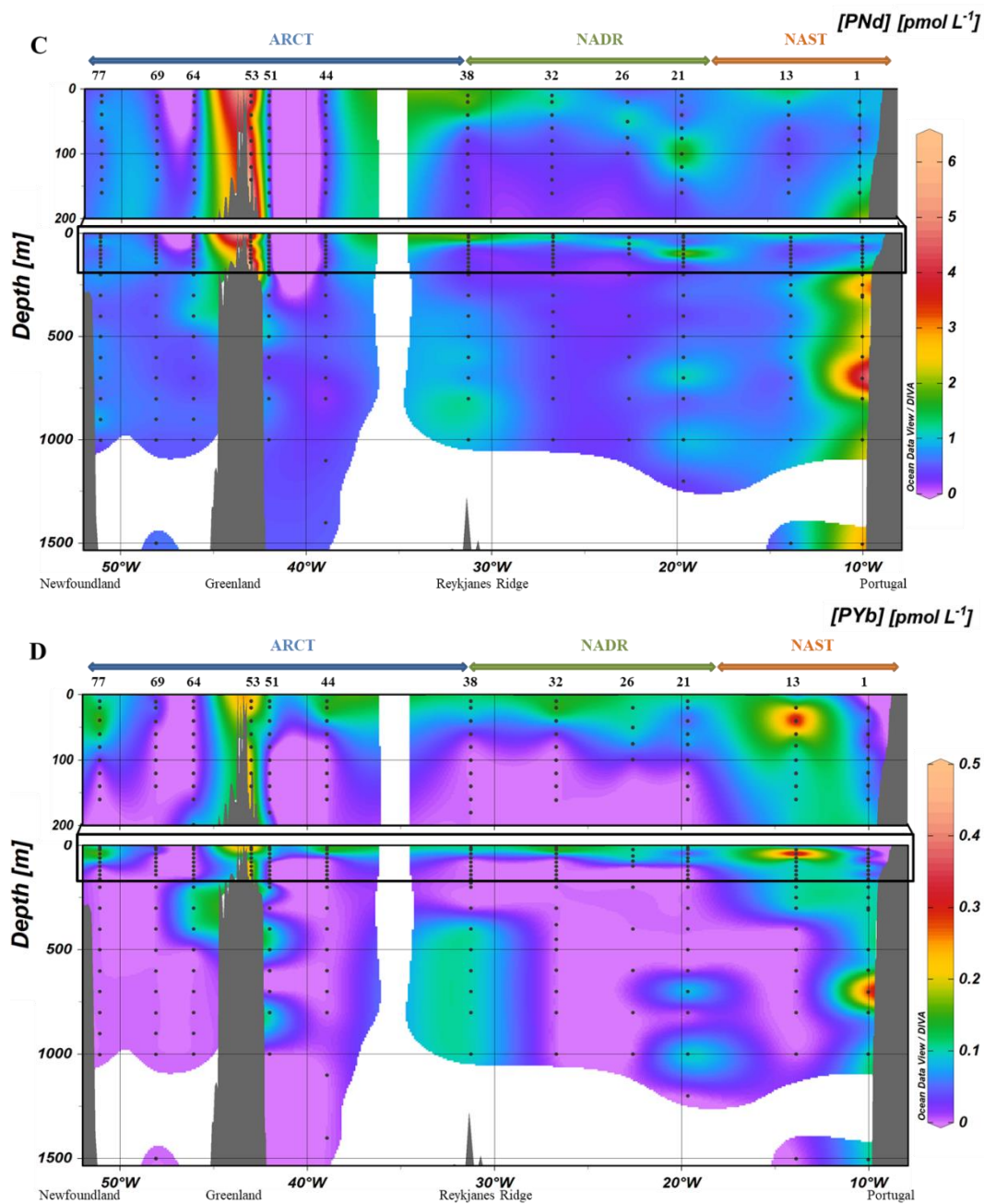
Figure 2: A. Vertical profiles of particulate [Ce] concentrations superimposed on salinity (S) measured by CTD at every GEOVIDE station (Lherminier and Sarthou, 2017); in white, the prevailing water masses characterized by a multiparametric (OMP) analysis: the Mediterranean Water (MW), the Subarctic Intermediate Water, the East North Atlantic Central Water (ENACW), the Subpolar Mode Water (SPMW), the Irminger Subpolar Mode Water (IrSPMW) and the Labrador Sea water (LSW) (García-Ibáñez et al., 2018). For the station #53, profiles are shifted to the bottom at a lower scale because of the shallow depth of the station. This map and the following were created with the software Ocean Data View (Schlitzer, 2016). B. Particulate [Ce] concentrations interpolated with the DIVA gridding function of Ocean Data View along the section defined in Fig. 1, with a zoom in the first 200 m in the upper panel.

845



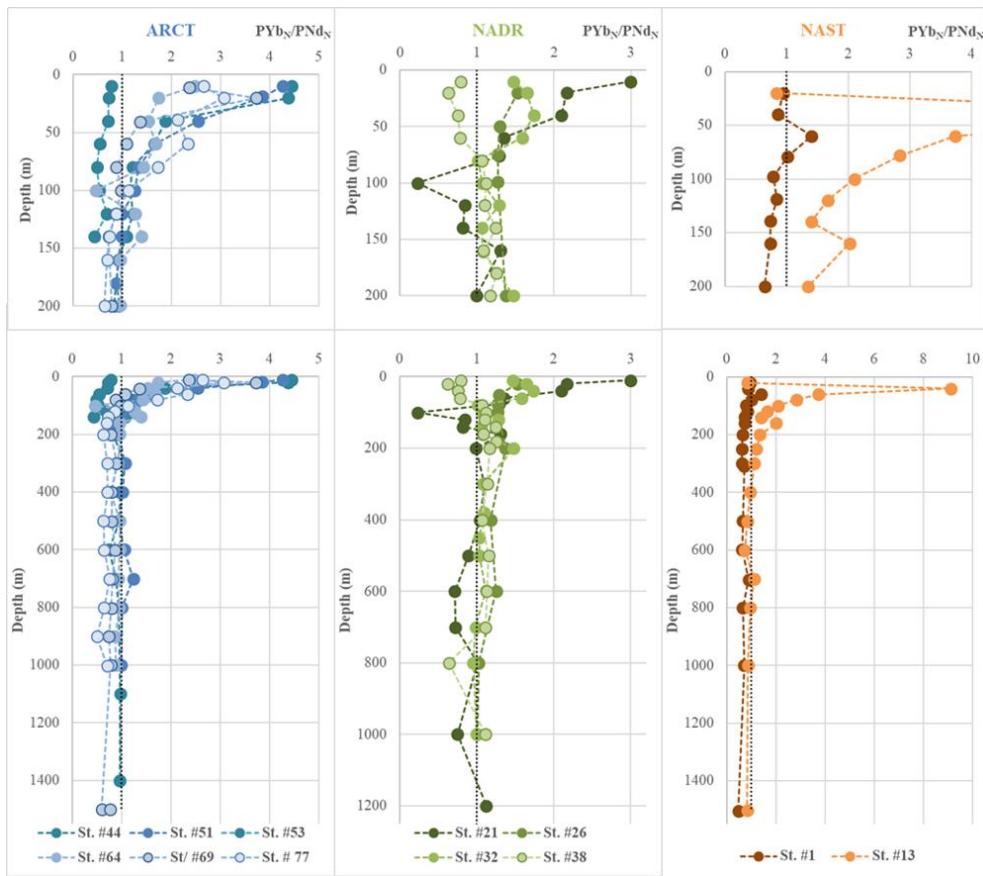
850



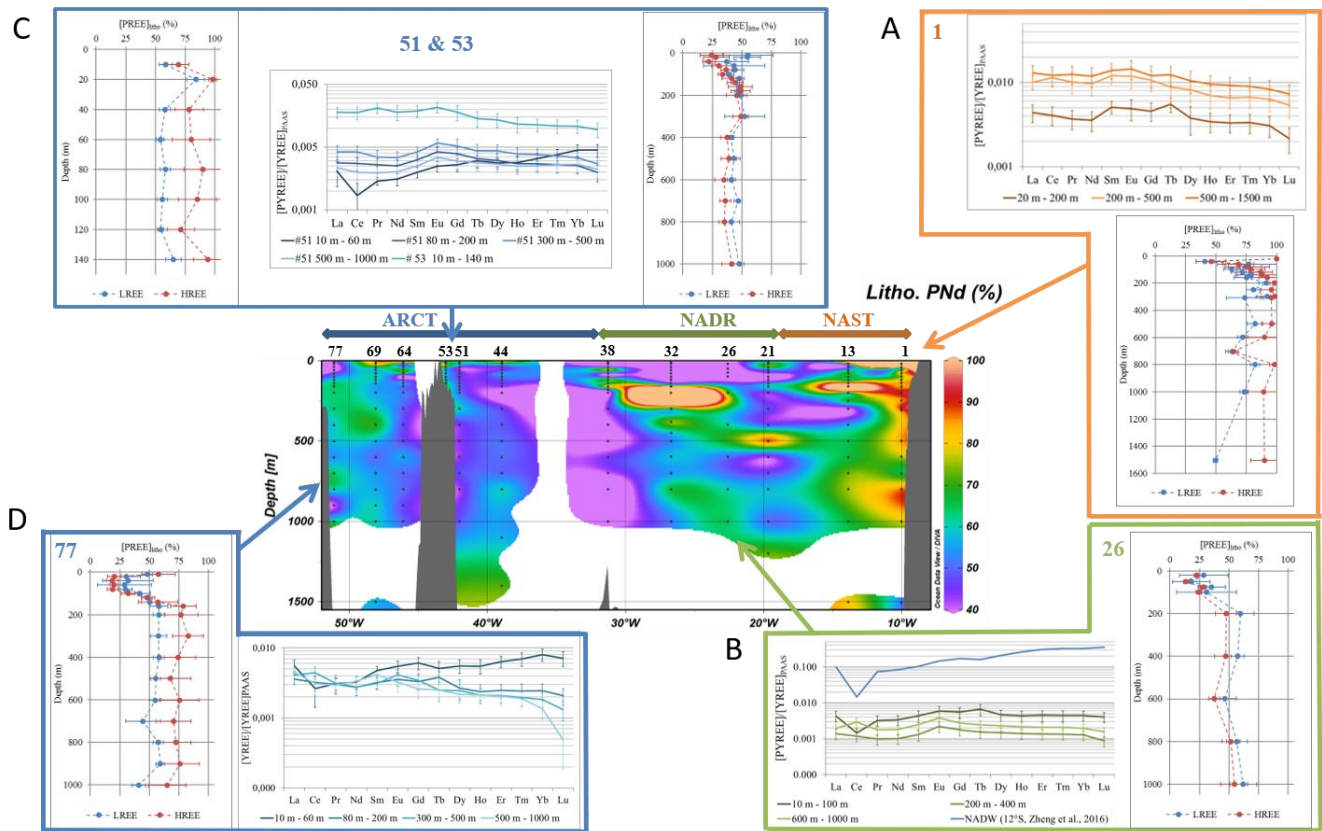


855 **Figure 3: A. Vertical profiles of particulate [Nd] and B. [Yb] concentrations superimposed on salinity (S) measured by CTD at every GEOVIDE station (Lherminier and Sarthou, 2017); in white, the prevailing water masses characterized by a multiparametric (OMP) analysis as in Fig. 2. At station #53, profiles are shifted to the bottom at a lower scale because of the shallow depth of the station. C. Particulate [Nd] and D. [Yb] concentrations interpolated with the DIVA gridding function of Ocean Data View along the section defined in Fig. 1., with a zoom on the first 200 m in the upper panel.**

860



865 **Figure 4: Vertical profiles of PYb/PNd ratios normalized to PAAS in each biogeochemical province (ARCT, NADR, NAST). The upper panels present the first 200 m and lower panels all the data. The dashed black vertical line on each panel represents a ratio equal to the one of PAAS.**



870 **Figure 5: Center: fraction of lithogenic PNd along the GEOVIDE section (in %); Side plots: vertical profiles of the lithogenic fraction of LREE (except Ce, blue lines) and HREEs (red lines) and PAAS-normalized REE patterns of the total fraction at stations A. #1, B. #26 C. #51 and #53 and C. #77 Patterns are averaged by depth intervals displaying similar values. Error bars represent the standard deviation of the concentration series. A typical seawater pattern (NADW; 12°S, 2499m, Zheng et al., 2016) is represented along with patterns of station #26 with a blue line.**

875

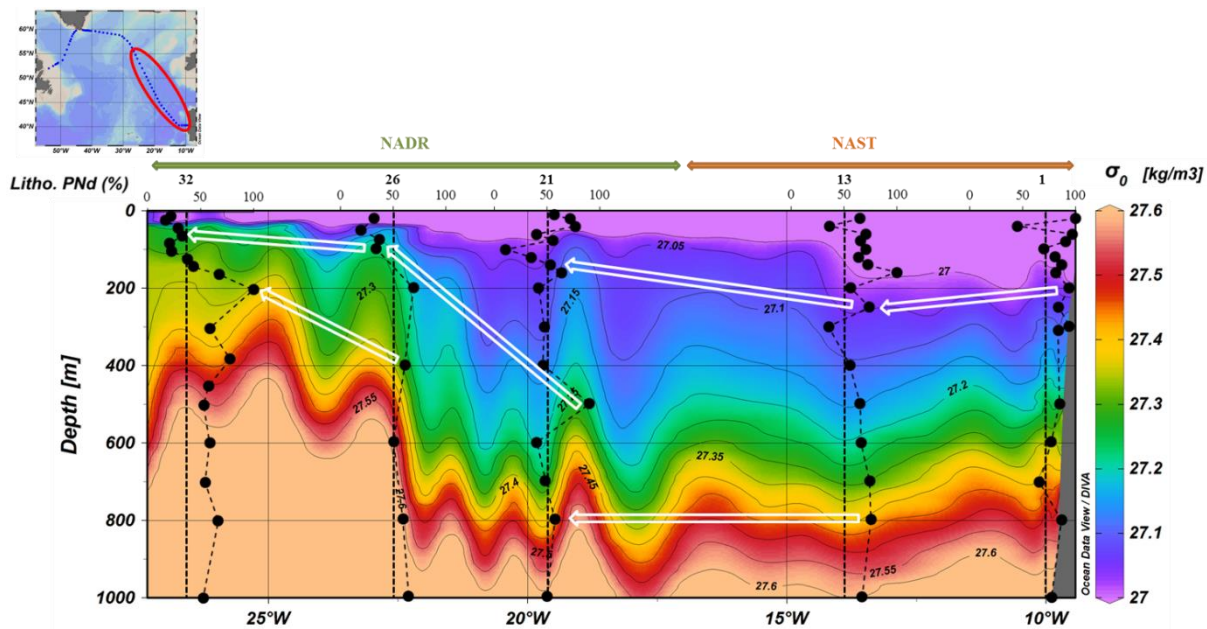
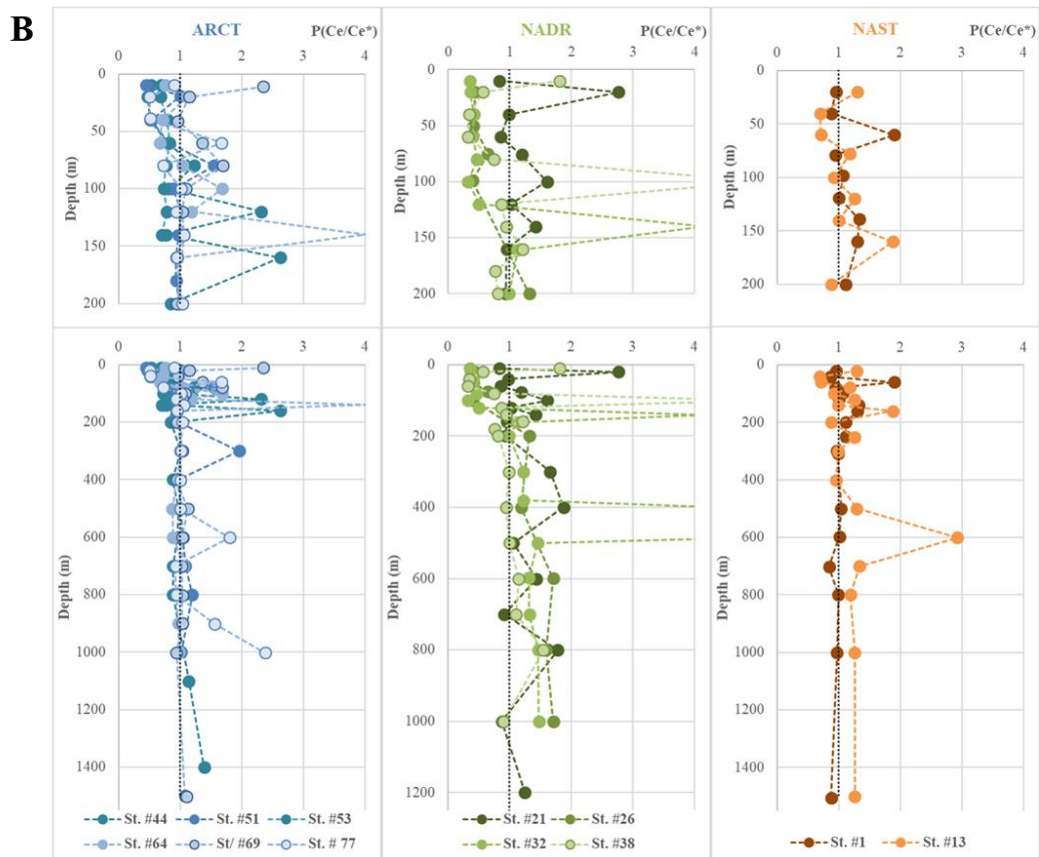
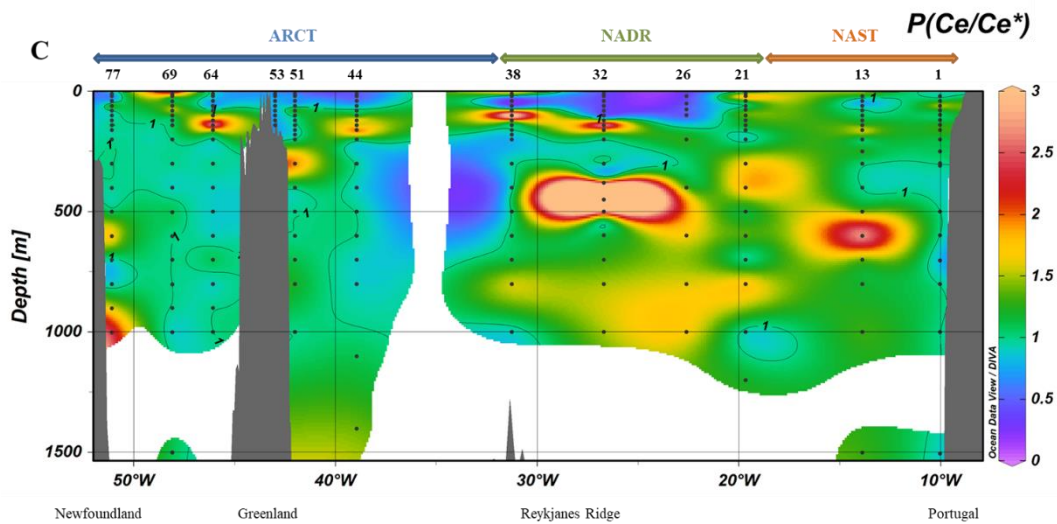
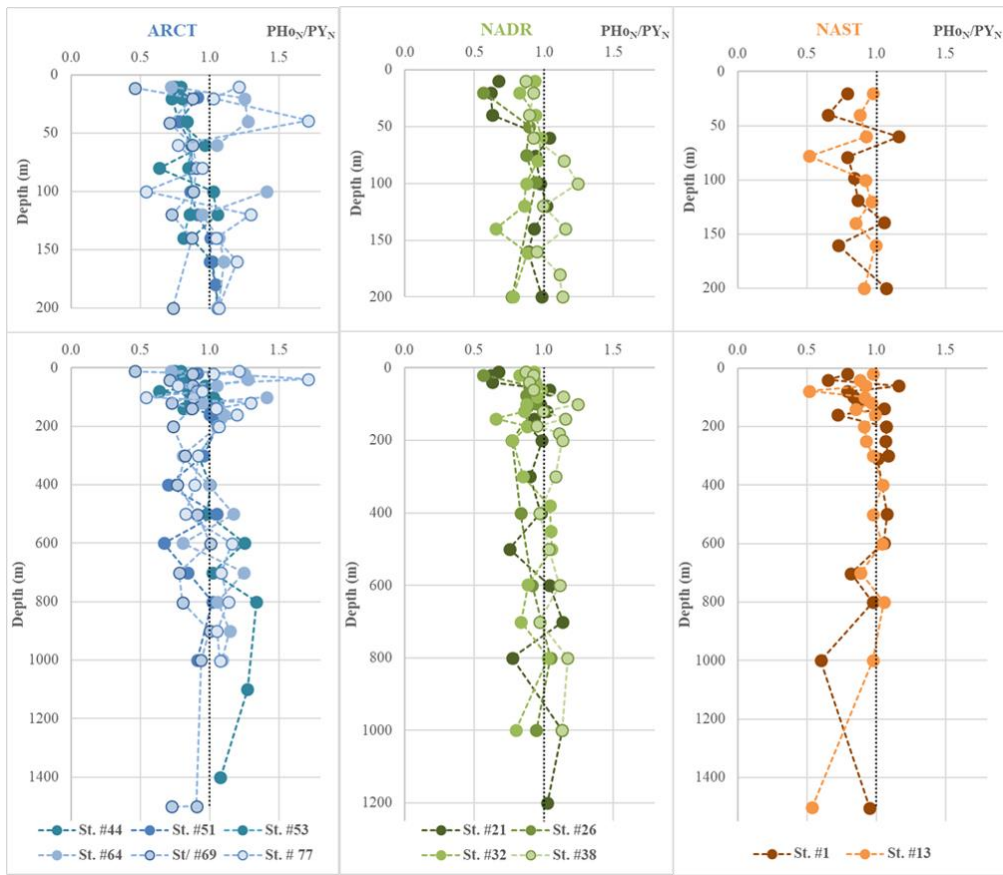


Figure 6: Estimated fraction of lithogenic PNd in the upper 1000m superimposed to density from station #1 to #32. White arrows follow the high lithogenic fractions spreading along the isopycnals  $\sigma_0=27.05$  and  $\sigma_0=27.4$ .

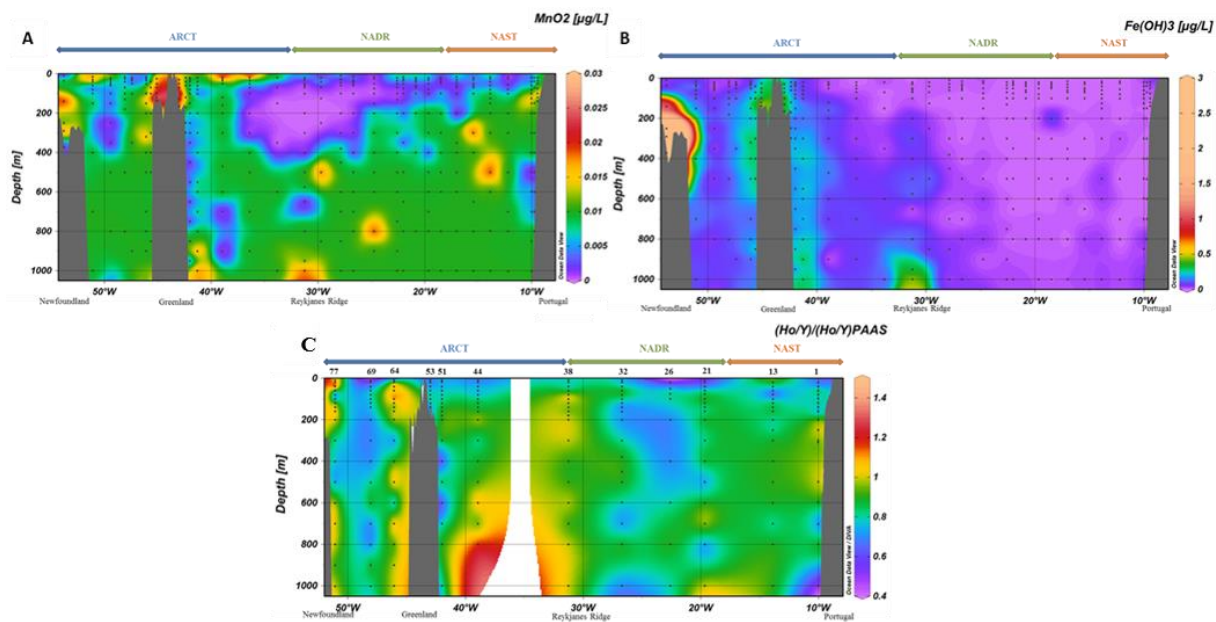
880



885 **Figure 7: A. Particulate Ce anomaly ( $\text{Ce}/\text{Ce}^*$ ) along the GEOVIDE section, interpolated with the DIVA gridding function of Ocean Data View and B.  $\text{Ce}/\text{Ce}^*$  profiles grouped by biogeochemical provinces (ARCT, NADR, NAST). The upper panels present the first 200 m and lower panels all the data. Values above 2.5 are not represented. The dashed black vertical line on each panel represents the absence of anomaly (1).**



**Figure 8: PAAS-normalized PHo/PY profiles grouped by biogeochemical provinces (ARCT, NADR, NAST). The upper panels present the first 200 m and lower panels all the data. The dashed black vertical line on each panel represents the PAAS-ratio (1).**



895

**Figure 9: A.  $MnO_2$  and B.  $Fe(OH)_3$  concentrations (in  $\mu g.L^{-1}$ ) calculated with the formula proposed by Lam et al. (2017) using particulate Mn, Fe and Al concentrations from Gourain et al. (2019). C. P<sub>Ho</sub>/P<sub>Y</sub> normalized to PAAS.**

900 **Author contribution**

N.L. did the sampling during the cruise, helped by C.J and H.P. N.L. did the leaching on the PC filters and conducted first Ba measurements. C.J., M.B., M.G. and M.L. did REE measurements. M.L. wrote the manuscript, corrected by C.J., H.P., M.G., N.L. and P.L.

**Competing interests**

The authors declare that they have no conflict of interest.

905